Structural Engineering and Mechanics, *Vol. 75, No. 5 (2020) 541-557*
DOI: https://doi.org/10.12989/sem.2020.75.5.541

A dissipative family of eigen-based integration methods for nonlinear dynamic analysis

Shuenn-Yih Chang*

Department of Civil Engineering, National Taipei University of Technology, 1, Section 3, Jungshiau East Road, Taipei 106-08, Republic of China

(Received July 8, 2019, Revised October 1, 2020, Accepted March 15, 2020)

Abstract. A novel family of controllable, dissipative structure-dependent integration methods is derived from an eigen-based theory, where the concept of the eigenmode can give a solid theoretical basis for the feasibility of this type of integration methods. In fact, the concepts of eigen-decomposition and modal superposition are involved in solving a multiple degree of freedom system. The total solution of a coupled equation of motion consists of each modal solution of the uncoupled equation of motion. Hence, an eigen-dependent integration method is proposed to solve each modal equation of motion and an approximate solution can be yielded via modal superposition with only the first few modes of interest for inertial problems. All the eigen-dependent integration methods combine to form a structure-dependent integration method. Some key assumptions and new techniques are combined to successfully develop this family of integration methods. In addition, this family of integration methods can be either explicitly or implicitly implemented. Except for stability property, both explicit and implicit implementations have almost the same numerical properties. An explicit implementation is more computationally efficient than for an implicit implementation since it can combine unconditional stability and explicit formulation simultaneously. As a result, an explicit implementation is preferred over an implicit implementation. This family of integration methods can have the same numerical properties as those of the WBZ-α method for linear elastic systems. Besides, its stability and accuracy performance for solving nonlinear systems is also almost the same as those of the WBZ-α method. It is evident from numerical experiments that an explicit implementation of this family of integration methods can save many computational efforts when compared to conventional implicit methods, such as the WBZ-α method.

Keywords: an eigen-based theory, unconditional stability, numerical damping, accuracy, structure-dependent coefficient

1. Introduction

When conducting dynamic response analyses of linear elastic structures, mode superposition is a useful technique for reducing computational efforts. This is because that the dynamic response of a structure can be reliably approximated by a superposition of a small number of the eigenmodes. In fact, good approximate solutions can be yielded via mode superposition with only first few mode shapes (Clough and Penzien 2003). Similarly, it is not necessary to accurately integrate all vibration modes to achieve an accurate solution in the time integration of inertial problems. In fact, a reliable solution can be obtained if the low frequency responses are accurately integrated while there exists no instability for high frequency modes. It is well recognized that a total solution is generally dominated by low frequency responses while high frequency responses contribute insignificantly for an inertial problem. Thus, a dissipative integration method is best suited to solving inertial problems since numerical damping can be applied to filter out the unimportant high frequency modes (Belytschko and Hughes 1983, Har and Tamma 2012). In general, the concept of mode superposition is also implied by conventional integration methods (Park 1975, Chang and Mahin 1993, Armero and Romero 2001, Chang 2001, Civalek 2007, Gao *et al*. 2012, Hadianfard 2012, Alamatian 2013, Soares 2014, Su and Xu 2014, Shojaee *et al*. 2015, Wen *et al*. 2017, Rezaiee-Pajand *et al*. 2018, Du et al. 2018, Kim and Lee 2018, Kim and Choi 2018, Kim 2019) and they use the same difference equations to solve each modal equation of motion. There is a great motivation to develop an integration method also based on a mode superposition concept but applying different difference equations to solve each modal equation of motion.

An eigen-based theory can be applied to develop a novel type of integration methods, where each modal equation of motion is solved by utilizing different displacement and/or velocity difference equations. This developing procedure is described next. In general, a coupled equation of motion for a multiple degree of freedom system can be uncoupled into a set of modal equations of motion. Next, an eigen-dependent integration method is proposed to solve each modal equation of motion, where the natural frequency of the modal equation of motion will be involved in developing an eigen-dependent integration method. Hence, coefficients of the displacement and/or velocity difference equations can be assumed to be functions of the product of natural frequency and step size. These eigen-dependent integration methods are required to reliably integrate low frequency modal equations of motion while no instability is guaranteed in solving high frequency modal equations of motion. Although a superposition of the eigenmodes can give the solution of the coupled equations of motion, it is

*Corresponding author, Professor
E-mail: changsy@ntut.edu.tw

Copyright © 2020 Techno-Press, Ltd.

ISSN: 1225-4568 (Print), 1598-6217 (Online)

time consuming for conducting an eigenvalue analysis for each time step for a system with a large number of degrees of freedom and also a mode superposition. As an alternative, all the eigen-dependent integration methods can be converted into a Structure-Dependent Integration Method (SDIM) by means of a reverse procedure for uncoupling the original equations of motion. As a result, these coefficients are no longer of eigen dependent but structure dependent and thus an eigenvalue analysis and a modal superposition of the eigenmodes of interest for each time step are avoided.

The numerical dissipation of an integration method is helpful to deal with a system with unresolved high frequency modes induced by spatial discretization since it can be used to reduce or eliminate the spurious growth of high frequency modes. Besides, the use of numerical damping to filter out the spurious oscillations of the high frequency modes in the solution of nonlinear problems can improve the convergence of nonlinear iterations. Consequently, it is preferable for an integration method to have numerical damping for solving inertial problems. Many integration methods with favorable numerical damping have been proposed for time integration, such as the Wilson-θ method (Wilson *et al*. 1973), HHT-α method (Hilber *et al*. 1977), WBZ-α method (Wood *et al*. 1981), generalized-α method (Chung and Hulbert 1993), α-function method (Chang 1997), γ-function method (Chang 2000), and the methods developed by Zhou and Tamma (2004); Xing et al. (2019). Most of these methods are implicit methods except for the α-function method and γ-function method. Although these implicit methods can have unconditional stability and second order accuracy, they will involve nonlinear iterations for each time step, which is time consuming for large order matrices. Meanwhile, although the α-function method and γ-function method can combine an explicit formulation and desired numerical damping together, they are conditionally stable.

SDIMs can be found in the literature (Chang 2002, 2007, 2009, 2010, 2014b, 2015b, Chang *et al*. 2015, 2016, Gui *et al*. 2014, Tang and Lou 2017) although there is lack of a theoretical foundation to affirm their feasibility for nonlinear dynamic analysis. Some SDIMs were claimed that they were derived from a discrete control theory (Chen and Ricles 2008, Gui *et al*. 2015, Tang and Lou 2017). However, it is still lack of a theoretical basis and a fatal defect of weak instability is found (Chang 2015a, 2017, 2018a). Besides, some other drawbacks still exist in current SDIMs (2015a, Chang 2017, 2018a). Hence, a novel family of dissipative SDIMs will be developed by using an eigen-based theory, where two important considerations will be addressed. One is to affirm that an eigen-based theory can provide a solid theoretical basis for developing a general SDIM that can simultaneously combine unconditional stability and explicit formulation, and then the Dahlquist barrier can be overcome (Dahlquist 1956, 1963). The other is to present an improved family of SDIMs with adequately high frequency numerical damping. Notice that this development can be treated as a typical procedure for developing a dissipative SDIM. It will be also shown that the proposed family of SDIMs can be both explicitly and implicitly implemented although the development of this investigation is aimed at developing an explicit SDIM.

2. Eigen-dependent integration method

After decomposing the coupled equation of motion for a multiple degree of freedom system into a series of modal equations of motion, an eigen-dependent integration method can be applied to solve each modal equation of motion based on an eigen-based theory. A modal equation of motion or an equation of motion for a single degree of freedom system can be written as:

$$m\ddot{u} + c\dot{u} + ku = f \tag{1}$$

where m, c, k and f represent the generalized mass, viscous damping coefficient, stiffness and dynamic loading for a specific mode, respectively (Clough and Penzien 2003). An eigen-dependent integration method will be proposed to solve Eq. (1). Two prerequisites are considered for deriving this integration method. One is to have desired numerical damping and the other is to be a semi-explicit integration method, where an explicit displacement difference equation and an implicit velocity difference equation will be adopted. It is found from conventional integration methods that an asymptotic equation of motion is generally adopted for a dissipative integration method, such as the HHT-α method (Hilber *et al*. 1977), WBZ-α method (Wood *et al*. 1981) and generalized-α method (Chung and Hulbert 1993). Herein, the asymptotic equation of motion and the velocity difference equation adopted by the WBZ-α method are chosen for this development. In addition, an explicit displacement difference equation is assumed since this study is intended to propose a semi-explicit integration method. Thus, the eigen-dependent integration method can be written as:

$$\begin{aligned}
&(1-\alpha)ma_{i+1} + \alpha ma_i + cv_{i+1} + kd_{i+1} = f_{i+1} \\
&d_{i+1} = -\beta_1\left[\Omega_i^2 d_i + 2\xi\Omega_i(\Delta t)v_i\right] + d_i + \beta_2(\Delta t)v_i \\
&\qquad + \beta_3(\Delta t)^2 a_i + p_{i+1} \\
&v_{i+1} = v_i + (\Delta t)\left[(1-\gamma)a_i + \gamma a_{i+1}\right]
\end{aligned} \tag{2}$$

where d_i, v_i, a_i and f_i denote the nodal displacement, velocity, acceleration and external force at the i-th time step, respectively; $\Omega_i = \omega_i(\Delta t)$ and $\omega_i = \sqrt{k_i/m}$ is the natural frequency determined from the generalized stiffness at the end of the of i-th time step k_i and generalized mass m (Clough and Penzien 2003). Besides, the coefficients of α and γ are scalar constants while those of β_1, β_2 and β_3 are assumed to be eigen dependent. Clearly, the displacement difference equation is explicit since it involves no current step data for determining the current displacement d_{i+1}. On the other hand, the velocity difference equation is implicit since the determination of v_{i+1} will involve the current step data a_{i+1}.

The displacement difference equation as shown in Eq. (2) is assumed to be eigen-dependent and explicit. In the

pilot study, only the previous data, i.e., the data at the i-th time step, are applied to determine an appropriate displacement difference equation and then a desired dissipative integration method. However, it cannot result in a family of integration methods that can have desired numerical properties. Hence, as an alternative, both the i-th and (i-1)-th step data are used to determine the difference equation. There is a great idea to replace the (i-1)-th step data with the i-th step data by using the asymptotic equation of motion. For this purpose, the term of $(\Delta t)^2 a_{i-1}$ is replaced by:

$$(\Delta t)^2 a_{i-1} = -\left[(1-\alpha)(\Delta t)^2 a_i + 2\xi\Omega_i(\Delta t)v_i + \Omega_i^2 d_i - F_i\right]/\alpha \quad (3)$$

As a result, $-\beta_1[\Omega_i^2 d_i + 2\xi\Omega_i(\Delta t)v_i]$ is introduced into the second line of Eq. (2). Notice that a loading-dependent term p_{i+1} is also adopted in this equation since it can be used to eliminate an amplitude growth in high frequency steady-state responses for an eigen-dependent integration method. The cause of this overshoot and the determination of the loading-dependent term for eigen-dependent or structure-dependent integration methods can be found in (Chang 2018a, b, c).

2.1 Determination of β_i

The determinations of the coefficients of β_1, β_2 and β_3 are the most important task of this development. Based on an eigen-based theory, low frequency modes must be accurately integrated while no numerical instability occur in high frequency modes. There is a possible way to meet these requirements by assuming that each of β_1, β_2 and β_3 is a fraction of Ω_0, where $\Omega_0 = \omega_0(\Delta t)$ and $\omega_0 = \sqrt{k_0/m}$ is the initial natural frequency of the mode and is determined from the initial generalized stiffness k_0 and generalized mass m. Besides, the numerator and denominator of β_1 to β_3 are assumed to be polynomial functions of Ω_0. As a result, they can be expressed as:

$$\beta_i = \frac{x_i + y_i 2\xi\Omega_0}{p + q2\xi\Omega_0 + r\Omega_0^2} \quad , \quad i = 1,2,3 \quad (4)$$

where p, q, r, x_i and y_i are scalar constants. An appropriate determination of β_i plays the key issue to successfully develop an eigen-dependent integration method. In unconditionally stable integration methods, low frequency modes are reliably integrated while instability is prohibited for high frequency modes. This prerequisite must be also met for SDIMs and is a fundamental basis for an eigen-based theory. Thus, low frequency modes must be integrated as accurately as a conventional integration method in the limit $\Omega_0 \to 0$. This can be achieved if β_i generally reduces to a constant and a nonzero constant term is adopted both in the numerator and denominator. Notice that an instability will experience if β_i becomes infinity in the limit $\Omega_0 \to \infty$. To avoid this condition, the maximum order of the polynomial of Ω_0 for the numerator must be no more than that of the denominator. Consequently, the denominator is assumed to be $D = 1 - \alpha + \gamma 2\xi\Omega_0 + \beta\Omega_0^2$ to simplify the determination of β_i, where ξ represents a viscous damping ratio. This assumption of D is referred to the implementation of the WBZ-α method. In addition, the numerator is assumed to be a linear polynomial function of Ω_0, i.e., $x_i + y_i 2\xi\Omega_0$.

Since a numerical method must be a convergent method, the satisfaction of convergence is required for the proposed eigen-dependent integration method. Thus, both consistency and stability must be satisfied based on the Lax equivalence theorem (Lax and Richmyer 1956). Consequently, they can be used to determine β_i. Besides, the proof of consistency relies upon the determination of the order of accuracy of the integration method and it can be determined from its local truncation error. Hence, based on the assumed formulation of β_i in Eq. (4), the local truncation error in correspondence to Eq. (2) for zero dynamic loading can be derived (Belytschko and Hughes 1983) and is found to be:

$$\begin{aligned}
E = {} & \frac{1}{BD}\left[(1-\alpha) - x_2\right]\ddot{u}_i \\
& + \frac{1}{BD}\left[\gamma - y_2 + (1-\alpha)\left(\gamma - \tfrac{1}{2} + \alpha\right)\right]2\xi\Omega_0\ddot{u}_i \\
& + \frac{1}{BD}\left[(1-\alpha) - x_2\right]2\xi\omega_0\dot{u}_i + \frac{1}{BD}(\gamma - y_2)2\xi\Omega_0 2\xi\omega_0\dot{u}_i \\
& - \frac{1}{BD}\left[x_1 - (1-\gamma)x_2 + x_3 + \alpha(1-\alpha)\right]\Omega_0\omega_0\dot{u}_i \\
& + \frac{1}{BD}\left[\alpha\gamma + \beta + y_1 - (1-\gamma)y_2 + y_3\right]2\xi\Omega_0\Omega_0\omega_0\dot{u}_i \\
& + \frac{1}{BD}\left[\gamma\left(\gamma - \tfrac{1}{2} + \alpha\right) - y_1\right]2\xi\Omega_0 2\xi\Omega_0\ddot{u}_i \\
& - \frac{1}{BD}y_1 2\xi\Omega_0 2\xi\Omega_0 2\xi\omega_0\dot{u}_i \\
& + \frac{1}{D}\left[-\left(\tfrac{1}{2} + \alpha\right)x_1 + \left(\tfrac{1}{2} - \tfrac{1}{2}\gamma\right)x_2 - \tfrac{1}{2}x_3 + \beta\right]\Omega_0^2\ddot{u}_i \\
& + \frac{1}{B}\tfrac{1}{6}2\xi\Omega_0(\Delta t)\dddot{u}_i + \frac{1}{B}\left(\tfrac{1}{12} + \tfrac{1}{2}\alpha\right)(\Delta t)^2\ddddot{u}_i + O\left[(\Delta t)^3\right]
\end{aligned} \quad (5)$$

where $B = 1 - \alpha + \gamma 2\xi\Omega_0$ is defined. In general, a second-order accurate integration method is of interest since it can be competitive to the other currently available integration methods. Thus, the coefficients of the terms that have an order of accuracy less than 2 must be equal to zero. As a result, some equalities can be obtained for determining x_i and y_i. One can easily find that $x_2 = 1 - \alpha$ and $y_2 = \gamma$. In addition, the following equations can be also obtained:

$$\begin{aligned}
& \gamma - y_2 + (1-\alpha)\left(\gamma - \tfrac{1}{2} + \alpha\right) = 0 \\
& x_1 - (1-\gamma)x_2 + x_3 + \alpha(1-\alpha) = 0 \\
& \alpha\gamma + \beta + y_1 - (1-\gamma)y_2 + y_3 = \gamma\left(\gamma - \tfrac{1}{2} + \alpha\right) - y_1
\end{aligned} \quad (6)$$

The first line of this equation will lead to $\gamma = \frac{1}{2} - \alpha$ after substituting $y_2 = \gamma$ into it. On the other hand, the adoption of $y_1 = 0$ can eliminate the term $-y_1 2\xi\Omega 2\xi\Omega 2\xi\omega\dot{u}_i/BD$. Since $y_1 = 0$ and $y_2 = \gamma$, it is straightforward to derive the result of $y_3 = \frac{1}{2}\gamma - \beta$ by using the third line of Eq. (5). In addition, after substituting

$x_2 = 1-\alpha$ into the second line of Eq. (6), one has $x_1 + x_3 = \frac{1}{2}(1-\alpha)$.

Apparently, the use of local truncation error is unable to determine all the coefficients of x_i and y_i. However, they can be further determined by using the other requirement to satisfy unconditional stability. In general, the characteristic equation of the amplification matrix $\mathbf{A}$ can be obtained from $|\boldsymbol{A} - \lambda \boldsymbol{I}| = 0$. Next, the limiting cases of $\Omega_0 \to \infty$ and $\Omega_0 \to 0$ will be examined. Thus, in the limit $\Omega_0 \to 0$, the characteristic equation is found to be:

$$\lambda^3 - A_1\lambda^2 + A_2\lambda - A_3 = 0 \tag{7}$$

where

$$\begin{aligned} A_1 &= 2 - \frac{\alpha}{1-\alpha} - \frac{(1-\alpha)(\gamma + x_1) + x_3}{(1-\alpha)\beta} \\ A_2 &= 1 - \frac{2\alpha}{1-\alpha} + \frac{(1-\alpha)(1-\gamma) - (1-2\alpha)x_1 - x_3}{(1-\alpha)\beta} \\ A_3 &= -\frac{\alpha}{1-\alpha} + \frac{\alpha x_1}{(1-\alpha)\beta} \end{aligned} \tag{8}$$

In general, λ_3 is a parasitic solution for Eq. (7) and the best choice is zero. The third line of this equation reveals that the choice of $x_1 = \beta$ will lead to $A_3 = 0$ and then $\lambda_3 = 0$. As a result, $x_3 = \frac{1}{2}(1-\alpha) - \beta$ is found. Thus, x_i and y_i are completely determined and the coefficients of β_1, β_2 and β_3 are found to be:

$$\begin{aligned} \beta_1 &= \frac{\beta}{D} \quad , \quad \beta_2 = \frac{1}{D}\left[(1-\alpha) + \gamma 2\xi\Omega_0\right] \\ \beta_3 &= \frac{1}{D}\left\{\left[\tfrac{1}{2}(1-\alpha) - \beta\right] - (\beta - \tfrac{1}{2}\gamma)2\xi\Omega_0\right\} \end{aligned} \tag{9}$$

On the other hand, after substituting the resultants of x_1 and x_3 into Eq. (8), the characteristic equation of Eq. (7) in the limit $\Omega_0 \to \infty$ can be simplified to be:

$$\left[\lambda^2 - \left(2 - \frac{1-\alpha}{\beta}\right)\lambda + \left(1 + \frac{\alpha}{\beta}\right)\right]\lambda = 0 \tag{10}$$

If this characteristic equation has a double root, it is very straightforward to obtain $\beta = \frac{1}{4}(1-\alpha)^2$. In addition, the two principal eigenvalues are found to be:

$$\lambda_{1,2} = 1 - \frac{1-\alpha}{2\beta} = -\frac{1+\alpha}{1-\alpha} \tag{11}$$

Since an unconditional stability requires that $|\lambda_i| \le 1$ for $i = 1,2,3$, thus the stability condition of $-\infty \le \alpha \le 0$ must be met. This conclusion can be manifested from Fig. 1, where the variations of the three eigenvalues with α are plotted.

Similarly, the characteristic equation corresponding to the limiting case of $\Omega_0 \to 0$ is found to be:

$$(\lambda - 1)^2\left(\lambda + \frac{\alpha}{1-\alpha}\right) = 0 \tag{12}$$

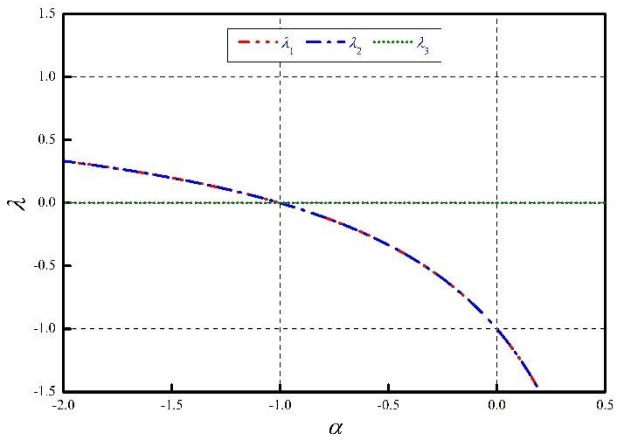

Fig. 1 Variations of eigenvalues of $\boldsymbol{A}$ with α as Ω_0 tends to infinity

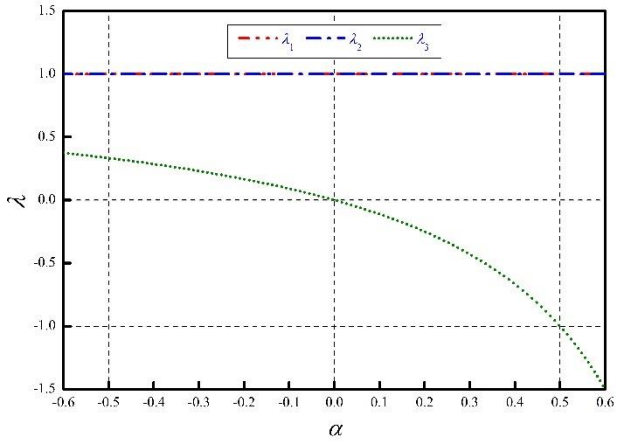

Fig. 2 Variations of eigenvalues of $\mathbf{A}$ with α as Ω_0 tends to zero

Clearly, the principal roots are $\lambda_{1,2} = 1$ and the spurious root is $\lambda_3 = -\alpha/(1-\alpha)$. The variations of the three roots with α are plotted in Fig. 2. This figure implies that the stability condition in the limit $\Omega_0 \to 0$ is $-\infty \le \alpha \le \frac{1}{2}$. Hence, the constraint on α for the limiting cases of $\Omega_0 \to 0$ and $\Omega_0 \to \infty$ is combined to be $-\infty \le \alpha \le 0$. This stability analysis in conjunction with a second order accuracy implies the convergence of the proposed family of the integration methods based on the Lax equivalence theorem (Lax and Richmyer 1956).

In summary, this proposed family of the eigen-dependent integration methods can have unconditional stability, second-order accuracy, and favorable numerical dissipation, which will be shown later, if the following relationships are chosen:

$$-\infty \le \alpha \le 0 \quad , \quad \beta = \tfrac{1}{4}(1-\alpha)^2 \quad \text{and} \quad \gamma = \tfrac{1}{2} - \alpha \tag{13}$$

This equation reveals that only a free parameter is involved for the subfamily of the proposed family of eigen-dependent integration methods. This family of integration methods is referred as the Chang Dissipative integration Method and is abbreviated as CDM for brevity. It will be

analytically shown and numerically corroborated later that CDM can be either explicitly or implicitly implemented for time integration and it may have different performance in the solution of nonlinear systems. Hence, CDM-E and CDM-I are adopted to denote Explicit and Implicit implementations of CDM, respectively. On the other hand, CDM is generally used to denote for both implementations. Notice that CDM-E will become the same as that of CDM-I for linear elastic systems.

2.2 Determination of p_{i+1}

It has been shown by Chang (2018c) that an appropriate loading-dependent term is needed in the displacement and/or velocity difference equations for general SDIMs so that an adverse overshoot in high frequency steady-state responses can be removed. Hence, the loading-dependent term p_{i+1} as shown in the second line of Eq. (2) must be appropriately determined. The root cause of this unusual amplitude growth and a remedy to overcome it has been investigated and thus the details will not be elaborated here again.

The technique to determine a loading-dependent term involves a local truncation error constructed from a non-homogeneous equation of motion. For this purpose, the local truncation error for CDM is found to be:

$$\begin{aligned} E = {} & \frac{1}{D}\left(\alpha+\gamma-\tfrac{1}{2}\right)\left[(\Delta t)\dddot{u}_i+\tfrac{1}{2}2\xi\Omega_0(\Delta t)\ddot{u}_i-\tfrac{1}{2}(\Delta t)^2\dddot{u}_i\right] \\ & +\frac{1}{D}\beta\Omega_0^2\dot{u}_i+\frac{1}{D}\left(\tfrac{1}{2}\alpha+\gamma-\tfrac{1}{2}\right)2\xi\Omega_0(\Delta t)\ddot{u}_i \\ & -\frac{1}{D}\tfrac{1}{12}(\Delta t)^2\dddot{u}_i+\frac{1}{BD}\beta\tfrac{1}{m}\left(f_{i+1}-f_i\right) \\ & +\frac{1}{BD}\beta\gamma 2\xi\Omega_0\tfrac{1}{m}\left(f_{i+1}-f_i\right)+\frac{1}{BD}\beta 2\xi\Omega_0\tfrac{1}{m}f_{i+1} \\ & -\left(p_{i+2}-2p_{i+1}+p_i\right)-\frac{1}{B}\left(1+\gamma 2\xi\Omega_0+2\xi\Omega_0\right)p_{i+1} \\ & +\frac{1}{B}\left(1+\gamma 2\xi\Omega_0\right)p_i+O\left[(\Delta t)^3\right] \end{aligned} \tag{14}$$

This equation reveals that CDM can generally have a first order accuracy for zero dynamic loading while it can have a second order accuracy if $\gamma=\frac{1}{2}-\alpha$ is adopted. On the other hand, for nonzero dynamic loading, it generally has a first order accuracy even if $\gamma=\frac{1}{2}-\alpha$ is taken. In addition, the term $\beta\Omega_0^2\ddot{u}_i/D$ is the only quadratic error term of Ω_0 as $\gamma=\frac{1}{2}-\alpha$ and it will result in an unusual overshoot in high frequency steady-state responses, which has been explored in the reference (Chang 2018c). It is required to determine an appropriate loading-dependent term p_{i+1} to eliminate the dominant error term $\beta\Omega_0^2\ddot{u}_i/D$ in the local truncation error. In fact, it can be removed by using the second derivative of the equation of motion:

$$\Omega_0^2\ddot{u}_i=\tfrac{1}{m}(\Delta t)^2\ddot{f}_i-\left[2\xi\Omega_0(\Delta t)\dddot{u}_i+(\Delta t)^2\ddot{u}_i\right] \tag{15}$$

where the quadratic term of Ω_0 is replaced by zero and linear order terms of Ω_0. Hence, a high frequency overshoot in steady-state responses can be removed. After substituting Eq. (15) into Eq. (14), one can choose an appropriate p_{i+1} to eliminate all the loading terms, whose order of accuracy is no more than 2. Consequently, the loading-dependent term is found to be:

$$p_{i+1}=\frac{1}{D}\beta\tfrac{1}{m}(\Delta t)^2\left(f_{i+1}-f_i\right)+\frac{1}{D}\beta\tfrac{1}{m}(\Delta t)^2 f_i \tag{16}$$

It is evident that the addition of the loading-dependent term in the displacement difference equation is intended to alter the local truncation error. In fact, Eq. (14) will be simplified to be:

$$\begin{aligned} E = {} & \frac{1}{D}\left(\alpha+\gamma-\tfrac{1}{2}\right)\left[(\Delta t)\dddot{u}_i+\tfrac{1}{2}2\xi\Omega_0(\Delta t)\ddot{u}_i-\tfrac{1}{2}(\Delta t)^2\dddot{u}_i\right] \\ & -\frac{1}{D}\left(\tfrac{1}{2}\alpha+\beta-\tfrac{1}{6}\right)2\xi\Omega_0(\Delta t)\ddot{u}_i-\frac{1}{D}\left(\beta-\tfrac{1}{12}\right)(\Delta t)^2\dddot{u}_i \\ & +O\left[(\Delta t)^3\right] \end{aligned} \tag{17}$$

Clearly, CDM has a second order accuracy if $\gamma=\frac{1}{2}-\alpha$ is chosen for any viscous damping and any dynamic loading.

A simple example is examined to confirm the importance of the inclusion of the term p_{i+1} in the formulation of CDM. For this purpose, the following problem is solved:

$$\ddot{u}+\omega_0^2u=\omega_0^2\sin\left(\bar{\omega}t\right) \tag{18}$$

where ω_0 is the natural frequency of the system; and $\bar{\omega}$ is the driving frequency of the sine loading. The theoretical solution of this equation is found to be:

$$u=\frac{1}{1-s^2}\sin\left(\bar{\omega}t\right)-\frac{s}{1-s^2}\sin\left(\omega_0 t\right) \tag{19}$$

where $s=\bar{\omega}/\omega_0$ is a ratio of frequency. For a small s or a high frequency mode, the response u is controlled by the steady-state response while it is governed by the transient response for a large s or a low frequency mode.

In these numerical illustrations, $\omega_0=10^3$ and $\bar{\omega}=0.5$ rad/s are specified and thus $s=5\times10^{-4}$ is found. Clearly, the solution of u is governed by the steady-state response since s is small. It can be determined from Eq. (18) that the asymptotic value of u is $sin(\bar{\omega}t)$ in the limit $s\to0$. This implies that an accurate solution can be obtained if the steady-state response is accurately integrated. It has been shown (Chang 2006) that a harmonic load can be accurately seized if $\Delta t/\bar{T}\le\frac{1}{12}$ is met, where $\bar{T}$ is the period of the harmonic load. Eq. (18) is solved by using CDM with $\alpha=0$ and -0.5, either without or with the loading-dependent term p_{i+1}. The time step of $\Delta t=1s$ is chosen to carry out time integration and it is small enough to accurately calculate the steady-state solution since the value of $\Delta t/\bar{T}$ is as small as $1/(4\pi)\le\frac{1}{12}$. The results are plotted in Fig. 3. An overshoot is found in Figs. 3(a) and 3(b) for both members of CDM if there exists no loading-dependent term. Hence, it is affirmed that a high frequency overshoot will appear in steady-state responses if

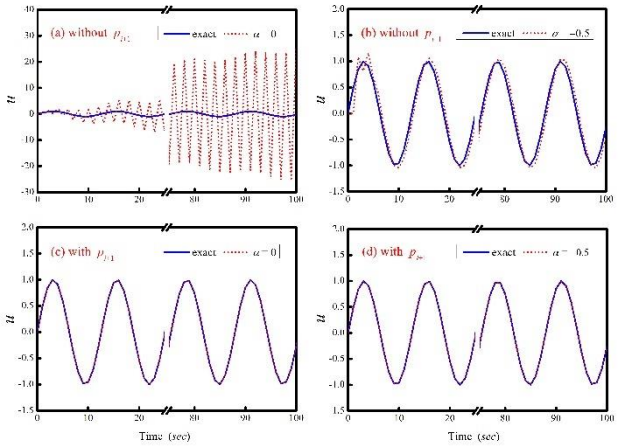

Fig. 3 Forced vibration responses of SDOF system for using CDM

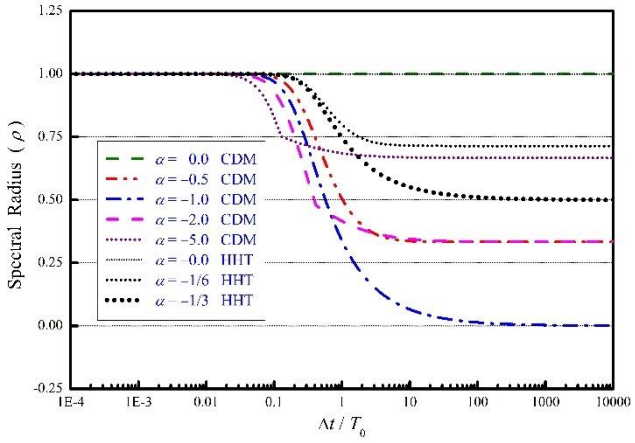

Fig. 4 Variation of spectral radius with $\Delta t / T_0$

a loading-dependent term is excluded from the displacement difference equation for a SDIM. In contrast, it can be seen in Figs. 3(c) and 3(d) that the results obtained from both members of CDM with the loading-dependent term almost overlap with the exact solution. Consequently, it is evident that the loading-dependent term p_{i+1} for CDM is capable to eliminate the high frequency overshoot in steady-state responses. Hence, it is substantiated that an appropriate loading-dependent term must be included in the difference equation for a SDIM.

3. Constraint on free parameter α

Numerical properties of CDM can be obtained from the eigen-analysis of its amplification matrix. The application of CDM to solve the free vibration response to a linear elastic single degree of freedom system can be written in a recursive matrix form as:

$$\mathbf{X}_{i+1} = \mathbf{A}\mathbf{X}_i \tag{20}$$

where $\boldsymbol{X}_{i+1} = [d_{i+1} \quad (\Delta t)v_{i+1} \quad (\Delta t)^2 a_{i+1}]^T$ is defined; $\mathbf{A}$ is an amplification matrix and it is invariant for a completely integration procedure for linear elastic systems. The explicit expression of $\mathbf{A}$ is found to be:

$$\mathbf{A} = \frac{1}{D}\begin{bmatrix} A_{11} & \beta_2 D & \beta_3 D \\ -\gamma\Omega_0^2 & A_{22} & 1-\alpha-\gamma+\left(\beta-\frac{1}{2}\gamma\right)\Omega_0^2 \\ -\Omega_0^2 & -\left(2\xi\Omega_0+\Omega_0^2\right) & A_{33} \end{bmatrix} \tag{21}$$

where the terms of $A_{11} = (1-\beta_1\Omega_0^2)D$, $A_{22} = 1-\alpha+(\beta-\gamma)\Omega_0^2$ and $A_{33} = -\left[\alpha+(1-\gamma)2\xi\Omega_0+\left(\frac{1}{2}-\beta\right)\Omega_0^2\right]$ are specified. The characteristic equation of $\mathbf{A}$ can be also expressed as that shown in Eq. (7) except that the coefficients for a general value of Ω_0 are found to be:

$$\begin{aligned} A_1 &= 2-\frac{1}{D}\left[\alpha+2\xi\Omega_0+\left(\gamma+\tfrac{1}{2}\right)\Omega_0^2\right] \\ A_2 &= 1-\frac{1}{D}\left[2\alpha+2\xi\Omega_0+\left(\gamma-\tfrac{1}{2}\right)\Omega_0^2\right] \\ A_3 &= -\frac{1}{D}\alpha \end{aligned} \tag{22}$$

The constraints on α, β and γ as shown in Eq. (13) are simply derived from the limiting cases of $\Omega_0 \to 0$ and $\Omega_0 \to \infty$. More rigorous constraints can be further derived if a general value of Ω_0 is considered. For this purpose, the eigenvalues of the matrix $\mathbf{A}$ for a general Ω_0 are found and explored. The spectral radius of $\mathbf{A}$ can be determined from $\rho = max(|\lambda_1|, \ |\lambda_2|, \ |\lambda_3|)$. Variations of spectral radii with $\Delta t/T_0$ are displayed in Fig. 4 for CDM with different α values. Fig. 4 reveals that the spectral radius is always less than or equal to unity for each curve. Thus, it is indicated that CDM can have an unconditional stability in the range of $-\infty \le \alpha \le 0$ for a linear elastic system. Each curve shows that the spectral radius ρ is 1 for small $\Delta t/T_0$ while it will become a certain constant when $\Delta t/T_0$ is large enough, say 100. It is seen that the α value in the range of $-1 \le \alpha \le 0$ leads to $0 \le \rho \le 1$ while that in $-\infty \le \alpha \le -1$ it results in $-1 \le \rho \le 0$. At first glance, it seems that CDM can provide a controllable numerical damping as α either in the range of $-1 \le \alpha \le 0$ or $-\infty \le \alpha \le -1$. However, the curve corresponding to α in the range of $-\infty \le \alpha \le -1$, such as $\alpha = -2$ and -5 in Fig. 4, exhibits an abrupt change of slope. Consequently, it is of interest further study the cause of this abrupt change.

Instead of plotting the variation of spectral radius with $\Delta t / T_0$, the variations of the real and imaginary parts of each principal root with $\Delta t/T_0$ for CDM are plotted in Fig. 5, where the calculated results for $\alpha = 0$, -0.5 and -1 are shown in Figs. 5(a) and 5(b) while those for $\alpha = -2$ and -5 are plotted in Figs. 5(c) and 5(d). It is seen in Fig. 5(b) that the imaginary part of the two principal roots is nonzero for CDM with $\alpha = 0$, -0.5 and -1.0. Thus, these members of CDM can have two complex conjugate eigenvalues for any $\Delta t/T_0$ and they will lead to an oscillatory response. On the other hand, Fig. 5(d) reveals that the imaginary part of the two principal roots will become zero after a certain value of $\Delta t/T_0$ for CDM with $\alpha = -2$ and -5. Hence, it is implied that the two complex conjugate eigenvalues will bifurcate into two distinct, real eigenvalues and they will result in a response in an exponential decay. Hence, it can be drawn that CDM with a α value in $-1 \le \alpha \le 0$ is preferred. As a result, Eq. (13) is modified to be:

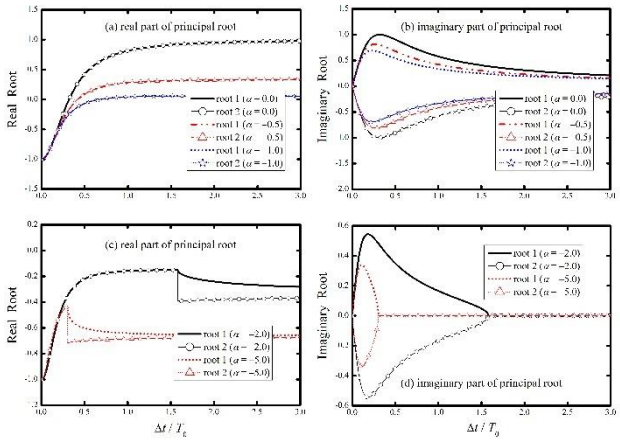

Fig. 5 Principal roots of CDM-E with different α values

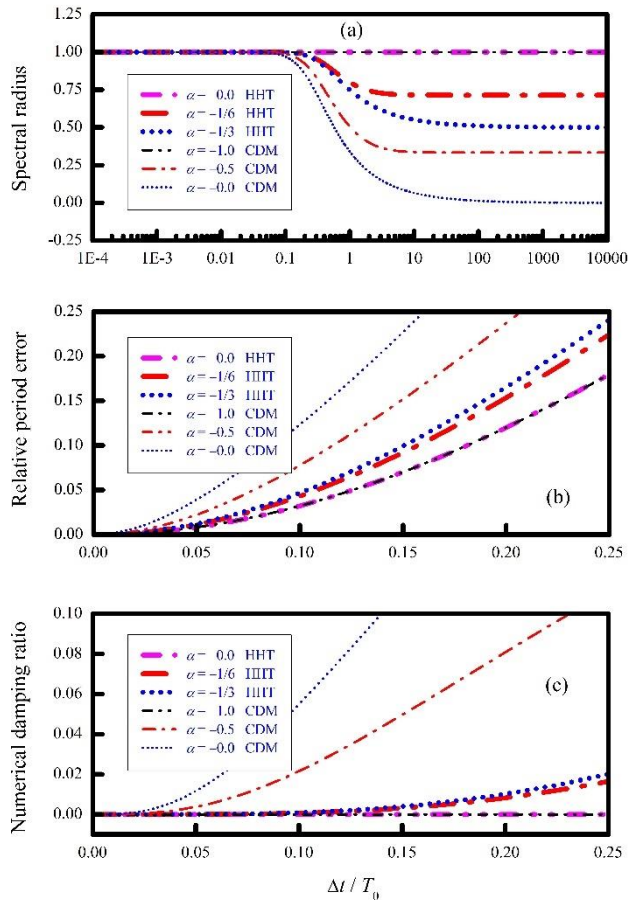

Fig. 6 Comparisons of numerical properties between HHT and CDM

$$-1 \le \alpha \le 0 \quad , \quad \beta = \tfrac{1}{4}(1-\alpha)^2 \quad \text{and} \quad \gamma = \tfrac{1}{2} - \alpha \qquad (23)$$

The relationships defined in this equation for the parameters of α, β, γ are strongly recommended for using CDM in practical applications.

It is of great interest to compare the numerical properties of CDM to those of the conventional dissipative integration method, such as HHT, since CDM is a dissipative integration method. For this purpose, the variations of spectral radius, relative period error and numerical damping ratio versus $\Delta t / T_0$ are plotted in Fig. 6. Notice that $-\frac{1}{3} \le \alpha \le 0$ is in correspondence to the spectral radius of $\frac{1}{2} \le \rho_\infty \le 1$ in the limit $\Omega_0 \to \infty$ for HHT while $-1 \le \alpha \le 0$ corresponds to $0 \le \rho_\infty \le 1$ for CDM. It is found that the member of $\alpha = 0$ for HHT and CDM has a unit spectral radius, zero numerical damping and the smallest relative period error since this degenerate member of the both integration methods is the constant average acceleration method. HHT with $\alpha = -\frac{1}{3}$ and CDM with $\alpha = -1$ possess the largest high frequency numerical damping of each integration method. In general, each curve can have a unit spectral radius for small $\Delta t/T_0$; then it decreases gradually; and finally it becomes a constant value of $\rho_\infty = 0.5$ for HHT and $\rho_\infty = 0$ for CDM as can be seen in Fig. 6(a). Apparently, both integration methods can have desired numerical damping. In addition, CDM can have more high frequency numerical damping in contrast to HHT as shown in Fig. 6(c). It is revealed by Fig. 6(b) that the member of $\alpha = 0$ for both integration methods has the smallest relative period error since it possesses no numerical damping. In general, a period distortion will increase with the increase of numerical damping for each integration method.

4. Enlargement of stability range

After comparing the characteristic equation of CDM to that of the WBZ-α method, it is found that they possess the same characteristic equation for linear elastic systems. Thus, the numerical properties of CDM will be the same as those of the WBZ-α method if these properties are derived from the same characteristic equation. Although CDM can have the same numerical properties as those of the WBZ-α method for linear elastic systems it is of interest to further investigate its numerical properties in the solution of nonlinear systems. A parameter, which is referred as the instantaneous degree of nonlinearity, has been introduced for monitoring the stiffness change for a nonlinear system (Chang 2007). In general, it is the ratio of the stiffness at the end of the (i+1)-*th* time step over the initial stiffness and is $\delta_{i+1} = k_{i+1} / k_0$. Thus, $\delta_{i+1} = 1$ implies that the instantaneous stiffness at the end of the (i+1)-*th* time step is equal to the initial stiffness; the stiffness hardening $\delta_{i+1} > 1$ reveals that the instantaneous stiffness is larger than the initial stiffness at the end of the (i+1)-*th* time step; and it is revealed by the stiffness softening $0 < \delta_{i+1} < 1$ that the instantaneous stiffness is less than the initial stiffness. It has been found (Chang 2007) that an integration method derived from an eigen-based theory generally have unconditional stability as $\delta_{i+1} \le 1$ and only has conditional stability as $\delta_{i+1} > 1$. It will be shown later that CDM-E also shows this particular stability property. Hence, its application to time integration might be inconvenient or limited due to conditional stability for stiffness hardening systems.

A methodology of using a stability amplification factor σ to virtually enlarge an initial stiffness for a SDIM has

been applied to improve its stability property (Chang 2015c). This can be explained next. In general, CDM-E can have an unconditional stability as $\delta_{i+1} \le 1$. Thus, it is implied that an unconditional stability can be obtained if the instantaneous generalized stiffness k_{i+1} is equal to or less than the initial generalized stiffness k_0, i.e., $\delta_{i+1} \le 1$. This implies that an unconditional stability range will be altered if the initial generalized stiffness is modified from k_0 to σk_0. In fact, after this modification, an unconditional stability range will be altered from $k_{i+1} \le k_0$ to $k_{i+1} \le \sigma k_0$. Consequently, an unconditional stability range can be arbitrarily enlarged if σ is chosen to be greater than 1. Whereas, it will be shrunk if $0 < \sigma < 1$ is adopted.

Applying this methodology to amplify an unconditional stability range for CDM-E, the only change of its formulation is to modify the denominator of the coefficients β_1 to β_3 from $D = 1 - \alpha + 2\gamma\xi\Omega_0 + \beta\Omega_0^2$ to $\bar{D} = 1 - \alpha + 2\gamma\xi\Omega_0 + \beta\sigma\Omega_0^2$. In addition, the numerator p_{i+1} must be also modified to be:

$$p_{i+1} = \frac{1}{\bar{D}}\beta\sigma\tfrac{1}{m}(\Delta t)^2\left(f_{i+1} - f_i\right) + \frac{1}{\bar{D}}\beta\tfrac{1}{m}(\Delta t)^2 f_i \tag{24}$$

Apparently, this loading-dependent term is derived from the same way as that to derive the one shown in Eq. (15) by using $\bar{D}$ to replace D. Thus, the order of accuracy is unaffected by the addition of the amplification factor. There will be no change in the formulation of CDM-E if $\sigma = 1$ is adopted. Meanwhile, the numerical properties of CDM-E will be altered for $\sigma \ne 1$. Thus, the nonlinear performance of CDM-E must be further assessed. For a nonlinear system, its stiffness is no longer a constant and might vary for each time step and thus its amplification matrix $\mathbf{A}$ will vary accordingly. Thus, the amplification matrix $\mathbf{A}$ in Eq. (21) must be replaced by $\mathbf{A}_{i+1}$, which is the amplification matrix for the (i+1)-th time step. As a result, the explicit expression of $\mathbf{A}_{i+1}$ is found to be:

$$\mathbf{A}_{i+1} = \begin{bmatrix} 1-\beta_1\Omega_i^2 & \beta_2 - \beta_1 2\xi\Omega_i & \beta_3 \\ -\dfrac{1}{B}\gamma x & 1-\dfrac{1}{B}\gamma y & 1-\gamma-\dfrac{1}{B}\gamma(\alpha+z) \\ -\dfrac{1}{B}x & -\dfrac{1}{B}y & -\dfrac{1}{B}(\alpha+z) \end{bmatrix} \tag{25}$$

where $x = (1-\beta_1\Omega_i^2)\Omega_{i+1}^2$, $y = 2\xi\Omega_0 + \beta_2\Omega_{i+1}^2 - \beta_1 2\xi\Omega_i\Omega_{i+1}^2$, $z = (1-\gamma)2\xi\Omega_0 + \beta_3\Omega_{i+1}^2$ and $B = 1 - \alpha + \gamma 2\xi\Omega_{i+1}$ are specified for nonlinear system. Besides, the denominator of β_1 to β_3 is also modified to be $\bar{D}$ if a stability amplification factor is involved. Notice that $\Omega_i^2 = \delta_i\Omega_0^2$ and $\Omega_{i+1}^2 = \delta_{i+1}\Omega_0^2$. In addition, $\delta_i = \delta_{i+1}$ is also assumed in the subsequent study of nonlinear properties since the difference between δ_i and δ_{i+1} is small for the two consecutive time steps.

To substantiate that a stability amplification factor σ can effectively enlarge an unconditional stability range, the variation of the upper stability limit with the instantaneous degree of nonlinearity is plotted in Fig. 7 for both $\alpha = 0$ and –0.5. Since the upper stability limit will be infinite for unconditional stability, a part of the curve disappears from this figure. Fig. 7(a) shows that CDM-E with $\alpha = 0$ can possess unconditional stability in the range of $\delta_{i+1} \le \sigma$ for $\sigma = 1$, 2 and 3 while it will become conditionally stable in the range of $\delta_{i+1} > \sigma$ for different viscous damping ratios of $\xi = 0$, 0.1 and 0.2. It is also found that the upper stability limit in the conditionally stable range will decrease with the increase of δ_{i+1}. A very similar phenomenon is also found in Fig. 7(b) for $\alpha = -0.5$. However, it is seen that the stability amplification factor for CDM with $\alpha = -0.5$ can extend an unconditional stability range to be considerably larger than that of $\delta_{i+1} \le \sigma$ for CDM with $\alpha = 0$. In fact, it can be written as $\delta_{i+1} \le \bar{\sigma}$, where $\bar{\sigma} \ge \sigma$. Thus, it is affirmed that the stability amplification factor σ can effectively alter an unconditional stability range from $\delta_{i+1} \le 1$ to $\delta_{i+1} \le \sigma$; and a large σ will lead to a large unconditional stability range.

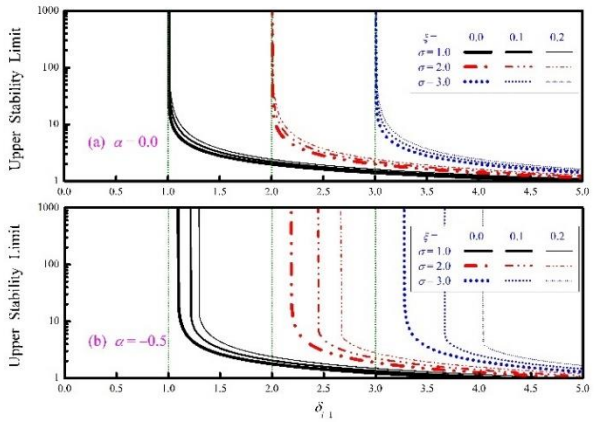

Fig. 7 Variation of upper stability limit with δ_{i+1} for $\alpha = 0$ and –0.5

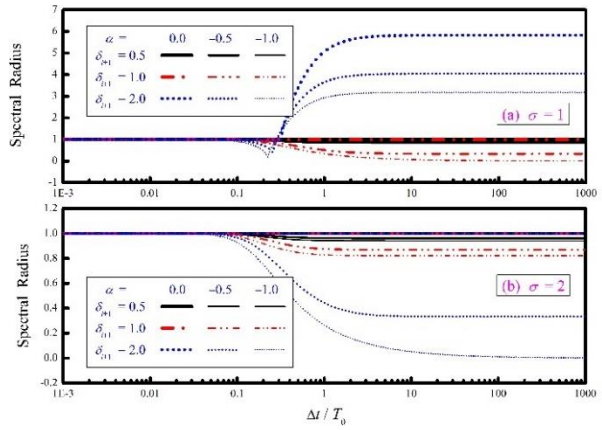

Fig. 8 Variation of spectral radius with $\Delta t/T_0$ for different α and δ_{i+1} values

As a summary, the final formulation of CDM can be, in general, expressed as:

$$\begin{aligned} &(1-\alpha)ma_{i+1} + \alpha ma_i + cv_{i+1} + kd_{i+1} = f_{i+1} \\ &d_{i+1} = \left(1-\beta_1\Omega_i^2\right)d_i + \left(\beta_2 - \beta_1 2\xi\Omega_i\right)(\Delta t)v_i \\ &\quad + \beta_3(\Delta t)^2 a_i + p_{i+1} \\ &v_{i+1} = v_i + (\Delta t)\left[(1-\gamma)a_i + \gamma a_{i+1}\right] \end{aligned} \tag{26}$$

where

$$\beta_1 = \frac{\beta}{\overline{D}} \quad , \quad \beta_2 = \frac{1}{\overline{D}}\left[(1-\alpha)+\gamma 2\xi\Omega_0\right]$$
$$\beta_3 = \frac{1}{\overline{D}}\left\{\left[\tfrac{1}{2}(1-\alpha)-\beta\right]-(\beta-\tfrac{1}{2}\gamma)2\xi\Omega_0\right\} \tag{27}$$
$$p_{i+1} = \frac{1}{\overline{D}}\beta\sigma\tfrac{1}{m}(\Delta t)^2(f_{i+1}-f_i)+\frac{1}{\overline{D}}\beta\tfrac{1}{m}(\Delta t)^2 f_i$$

The choices of the values α, β and γ for conducting time integration are recommended in Eq. (23).

5. Numerical properties

The numerical properties of CDM-E will be altered after introducing δ_{i+1} and σ into its original formulation. It is seen that the instantaneous stiffness of a real structure is very rare to be larger than twice of that of the initial stiffness, and thus $\delta_{i+1} \le 2$ is of practical significance. On the other hand, the choice of $\sigma = 2$ for CDM-E can have an unconditional stability range of $\delta_{i+1} \le 2$. Hence, $\sigma = 2$ is taken in the subsequent study. In the basic analysis of a nonlinear system, the Von Neuman assumption is adopted and is conducted only for the (i+1)-th time step but not for a whole integration procedure. However, this analysis can still provide a valuable information since an integration procedure consists of each time step. The general formulas for computing the relative period error and numerical damping ratio for nonlinear systems can be found in the references (Chang 2010, 2014a, 2015a) and will not be shown herein for brevity.

5.1 Stability

The variation of the spectral radius versus $\Delta t/T_0$ is shown in Fig. 8. In Fig. 8(a), the spectral radius is generally no more than 1 for $\delta_{i+1} \le 1$ and finally approaches a certain constant smaller than 1 while it will become greater than 1 after a certain value of $\Delta t/T_0$ for $\delta_{i+1} > 1$ and finally tends to a certain constant larger than 1. Whereas, in Fig. 8(b), the spectral radius is always less than or equal to 1 as $\delta_{i+1} \le 2$. This is consistent with the analytical prediction that the application of σ to CDM-E will enlarge the unconditional stability range from $\delta_{i+1} \le 1$ to $\delta_{i+1} \le \sigma$. In general, each curve, except for the cases of $\sigma = 1$ with $\delta_{i+1} = 2$, has a unit spectral radius for small $\Delta t/T_0$ while it will decrease gradually and finally tend to a certain constant smaller than 1. This indicates that CDM-E can have desired numerical dissipation.

5.2 Period distortion and numerical damping

The variations of relative period errors and numerical damping ratios with $\Delta t/T_0$ for $\sigma = 1$ and 2 are plotted in Fig. 9. In general, the period is elongated for CDM-E and increases with the increase of $\Delta t/T_0$ for the given α andδ_{i+1} values. It is revealed by either Fig. 9(a) or 9(c) that the three curves corresponding to $\delta_{i+1} = 0.5$, 1 and 2

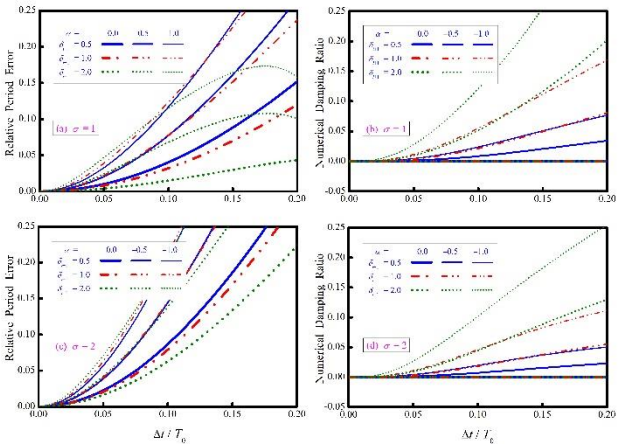

Fig. 9 Variation of relative period error and numerical damping with $\Delta t/T_0$ for different α and δ_{i+1}

seemingly cluster together for a given α value. It is also seen that the relative period error affected by α is more significant than that by δ_{i+1}. Notice that the decrease of α or δ_{i+1} will increase the period distortion. Comparing Figs. 9(a) to 9(c) for each curve, correspondingly, the relative period error for $\sigma = 2$ is, in general, larger than that of $\sigma = 1$ for a small value of $\Delta t/T_0$. In addition, numerical experiments also reveal that the increase of σ leads to the increase of period distortion for a small $\Delta t/T_0$. Thus, although a large value of σ can effectively enlarge an unconditional stability range from $\delta_{i+1} \le 1$ to $\delta_{i+1} \le \sigma$, it causes more period distortion. In general, the relative period error is small for $\Delta t / T_0 \le 0.05$ in both Figs. 9(a) and 9(c). Hence, CDM-E with either $\sigma = 1$ or $\sigma = 2$ can give an acceptable solution with comparable accuracy for a nonlinear system, if $\Delta t / T_0 \le 0.05$ is satisfied for the modes of interest. As a result, the choice of $\sigma = 2$ for CDM-E is recommended for practical applications based on both stability and accuracy considerations since CDM-E with $\sigma = 2$ can have an unconditional stability range of $\delta_{i+1} \le 2$ and a negligible period distortion as $\Delta t/T_0 \le 0.05$. On the other hand, the variations of numerical damping ratios with $\Delta t/T_0$ for CDM-E with $\sigma = 1$ and 2 are plotted in Figs. 9(b) and 9(d). In general, zero numerical damping can be achieved for $\alpha = 0$ for any δ_{i+1} for both $\sigma = 1$ and 2. Whereas, the numerical damping ratio generally increases with the increasing value of $\Delta t/T_0$. In addition, it also increases with decreasing σ for a given $\Delta t/T_0$. As a summary, a controllable numerical damping property can be generally obtained for CDM-E with an appropriate value of $\sigma \ge 1$ and the choice of $-1 \le \alpha \le 0$ if $\delta_{i+1} \le \sigma$ is met during the integration procedure.

5.3 Overshoot

An unusual overshoot, which shows an amplitude growth in contrast to an exact solution in the early transient response, has been found in an integration method although it can have unconditional stability (Goudreau and Taylor 1972). Hence, this property must be assessed in developing

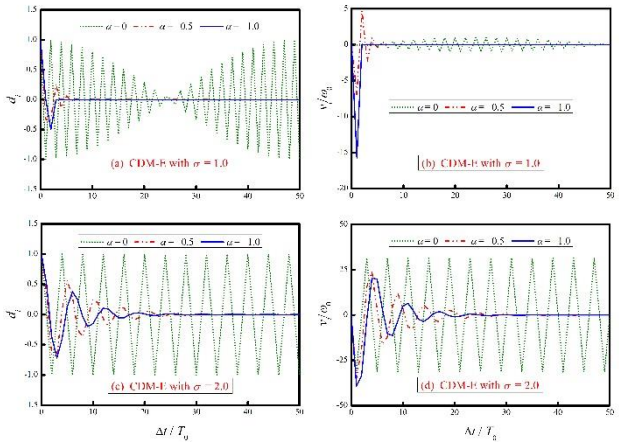

Fig. 10 Overshoot of CDM-E for linear elastic system

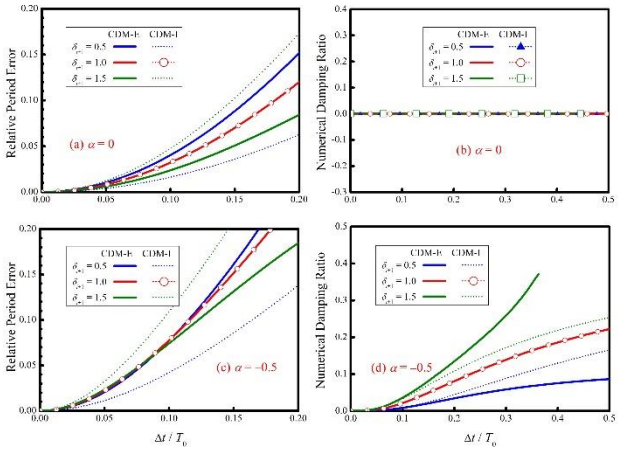

Fig. 11 Comparisons of numerical properties between CDM-E and CDM-I

an integration method. The overshooting potential of an integration method can be revealed by computing the discrete displacement and velocity in terms of initial conditions. The response behavior in the limit $\Omega_0 \to \infty$ can give an indication of the behavior of the high frequency modes (Hilber and Hughes 1978). As a result, the following equations can be obtained in the limiting case of $\Omega_0 \to \infty$:

$$\begin{aligned} d_{i+1} &\approx \left[1-\frac{\frac{1}{2}(1-\alpha)}{\beta\sigma}\right]d_i \\ v_{i+1} &\approx \left(\frac{\gamma}{2\beta\sigma}-1\right)\Omega_0\omega_0 d_i + \left(1-\frac{\gamma}{\beta\sigma}\right)v_i \end{aligned} \tag{28}$$

No overshoot in displacement is seen in the first line of this equation for CDM-E while a tendency to overshoot linearly in Ω_0 in the velocity equation is found in the second line due to the initial displacement term.

An example is examined to corroborate the analytical prediction of overshooting behavior for CDM-E. In fact, the free vibration response to the initial conditions of $d_0 = 1$ and $v_0 = 0$ for a single degree of freedom system is solved. A time step of $\Delta t = 10T_0$ is used for each dynamic analysis. The calculated results are plotted in Fig. 10. Notice that the velocity term is normalized by the initial natural frequency of the system in order to have the same unit as displacement. Figs. 10(a) and 10(c) show that there is no overshoot in the displacement response for CDM-E with $\alpha = 0$, -0.5 and -1 and for both $\sigma = 1$ and 2. Whereas, a significant overshoot in velocity is found in Figs. 10(b) and 10(d). Notice that the amount of overshoot in velocity for $\sigma = 2$ is greater than that of $\sigma = 1$, which is found after comparing Figs. 10(b) to 10(d). Hence, the overshoot phenomena both in displacement and velocity for CDM-E with $\alpha = 0$, -0.5 and -1 are in good agreement with the analytical results shown in Eq. (28).

6. Conversion

After the assessments of the numerical properties of the family of eigen-dependent integration methods for CDM-E, it is affirmed that it can accurately integrate low frequency modes while there is no instability for high frequency modes. Thus, it can satisfy the requirement for developing an eigen-dependent integration method according to an eigen-based theory. Conceptually, each modal equation of motion can be solved by an eigen-dependent integration method for a given natural frequency. However, it is impractical to compute each modal response and then to use a mode superposition method to obtain a total response. Alternatively, one can apply a reverse procedure of an eigen-decomposition technique to convert all the eigen-dependent integration methods, which correspond to all the eigenmodes of the coupled system, into a SDIM (Chang 2019). As a result, the family of SDIMs for CDM-E can be expressed as:

$$\begin{aligned} &(1-\alpha)\mathbf{M}\mathbf{a}_{i+1} + \alpha\mathbf{M}\mathbf{a}_i + \mathbf{C}_{i+1}\mathbf{v}_{i+1} + \mathbf{K}_{i+1}\mathbf{d}_{i+1} = \mathbf{f}_{i+1} \\ &\mathbf{d}_{i+1} = \left[\mathbf{M} - \mathbf{B}_1(\Delta t)^2\mathbf{K}_i\right]\mathbf{d}_i + \left[\mathbf{B}_2 - \mathbf{B}_1(\Delta t)\mathbf{C}_i\right](\Delta t)\mathbf{v}_i \\ &\qquad + \mathbf{B}_3(\Delta t)^2\mathbf{a}_i + \mathbf{p}_{i+1} \\ &\mathbf{v}_{i+1} = \mathbf{v}_i + (\Delta t)\left[(1-\gamma)\mathbf{a}_i + \gamma\mathbf{a}_{i+1}\right] \end{aligned} \tag{29}$$

where $\mathbf{M}$ is the mass matrix of the structural system; and $\mathbf{C}_{i+1}$ and $\mathbf{K}_{i+1}$ are the viscous damping coefficient and stiffness matrices, respectively, at the end of the (i+1)-*th* time step. In addition, $\mathbf{d}_i$, $\mathbf{v}_i$, $\mathbf{a}_i$ and $\mathbf{f}_i$ are the nodal vectors of the displacement, velocity, acceleration and external force, respectively. The coefficient matrices of $\mathbf{B}_1$ to $\mathbf{B}_3$ and the loading-dependent vector $\mathbf{p}_{i+1}$ are structure dependent and are found to be:

$$\begin{aligned} \mathbf{B}_1 &= \bar{\mathbf{D}}^{-1}\beta \\ \mathbf{B}_2 &= \bar{\mathbf{D}}^{-1}\left[(1-\alpha)\mathbf{M} + \gamma(\Delta t)\mathbf{C}_0\right] \\ \mathbf{B}_3 &= \bar{\mathbf{D}}^{-1}\left\{\left[\tfrac{1}{2}(1-\alpha)-\beta\right]\mathbf{M} - (\beta-\tfrac{1}{2}\gamma)(\Delta t)\mathbf{C}_0\right\} \\ \mathbf{p}_{i+1} &= \bar{\mathbf{D}}^{-1}\beta\left[\sigma(\Delta t)^2(\mathbf{f}_{i+1}-\mathbf{f}_i) + (\Delta t)^2\mathbf{f}_i\right] \\ \bar{\mathbf{D}} &= (1-\alpha)\mathbf{M} + \gamma(\Delta t)\mathbf{C}_0 + \beta\sigma(\Delta t)^2\mathbf{K}_0 \end{aligned} \tag{30}$$

where $\mathbf{K}_0$ is the initial tangent stiffness matrix and the stiffness matrix $\mathbf{K}_{i+1}$ at the (i+1)-*th* time step in the first

line of Eq. (29) is generally different from $\mathbf{K}_0$ for a nonlinear system. Notice that the restoring force vector $\boldsymbol{r}_{i+1}$ is often introduced to replace $\mathbf{K}_{i+1}\mathbf{d}_{i+1}$ in the step-by-step solution procedure. Since the coefficient matrices of $\mathbf{B}_1$ to $\mathbf{B}_3$ and the loading-dependent vector $\mathbf{p}_{i+1}$ are functions of $\boldsymbol{M}$, $\boldsymbol{C}_0$ and $\mathbf{K}_0$ as well as the step size, thus CDM-E becomes structure dependent after this transformation and is no longer eigen dependent.

7. Implementation

Unlike convention1al integration methods, a SDIM can be either an explicitly or implicitly implemented. For example, CDM can have an explicit implementation if the structure-dependent coefficients are kept invariant during a complete integration procedure. In contrast, it can be also implicitly implemented if these structure-dependent coefficients are updated with the change of the structural properties for each time step, where current structural properties are adopted to determine the structure-dependent coefficients. This can be explained next.

The second line of Eq. (29) can be applied to determine the displacement vector $\mathbf{d}_{i+1}$ and this solution procedure is numerically equivalent to solve the equation of:

$$\begin{aligned}\bar{\mathbf{D}}\left(\mathbf{d}_{i+1}-\mathbf{d}_i\right) &= -\beta\left(\Delta t\right)^2\mathbf{r}_i-\beta\left(\Delta t\right)^2\mathbf{C}_i\mathbf{v}_i \\ &+\left[\left(1-\alpha\right)\mathbf{M}+\gamma\left(\Delta t\right)\mathbf{C}_0\right]\left(\Delta t\right)\mathbf{v}_i \\ &+\left\{\left[\tfrac{1}{2}\left(1-\alpha\right)-\beta\right]\mathbf{M}-\left(\beta-\tfrac{1}{2}\gamma\right)\left(\Delta t\right)\mathbf{C}_0\right\}\left(\Delta t\right)^2\mathbf{a}_i\end{aligned} \tag{31}$$

After determining the displacement vector $\mathbf{d}_{i+1}$, the restoring force vector $\mathbf{r}_{i+1}$ in correspondence to $\mathbf{d}_{i+1}$ can be obtained from an assumed force-displacement relationship. Next, the velocity vector can be obtained from substituting the first line into the third line of Eq. (29) and is numerically equivalent to solve:

$$\begin{aligned}\left[\left(1-\alpha\right)\mathbf{M}+\gamma\left(\Delta t\right)\mathbf{C}_0\right]\mathbf{v}_{i+1} &= \gamma\left(\Delta t\right)\left(\mathbf{f}_{i+1}-\mathbf{r}_{i+1}\right)+\left(1-\alpha\right)\mathbf{M}\mathbf{v}_i \\ &+\left(1-\alpha-\gamma\right)\left(\Delta t\right)\mathbf{M}\mathbf{a}_i\end{aligned} \tag{32}$$

Finally, the equation of motion can be applied to determine the acceleration vector $\mathbf{a}_{i+1}$ and can be alternatively written as:

$$\left(1-\alpha\right)\mathbf{M}\mathbf{a}_{i+1}=\mathbf{f}_{i+1}-\alpha\mathbf{M}\mathbf{a}_i-\mathbf{C}_0\mathbf{v}_{i+1}-\mathbf{r}_{i+1} \tag{33}$$

A direct elimination method is generally adopted to solve Eqs. (31), (32) and (33). However, there is no need to employ a direct elimination method to solve Eq. (33) if $\mathbf{M}$ is a diagonal matrix. Similarly, Eq. (32) will involve no direct elimination methods if $\mathbf{M}$ is a diagonal matrix in addition to zero damping matrix. A direct elimination method consists of a triangulation and a substitution; and a triangulation consumes much more time than for a substitution. Notice that the triangulation of the matrix of $\bar{\boldsymbol{D}}$, $(1-\alpha)\boldsymbol{M}+\gamma(\Delta t)\boldsymbol{C}_0$ or $(1-\alpha)\mathbf{M}$ is needed to be done only once at the beginning of time integration since they remain invariant for a whole step-by-step integration procedure. This explains why a SDIM can be computationally efficient for the nonlinear dynamic analysis of inertial problems.

Apparently, Eqs. (31) and (32) will become nonlinear equations if the initial structural properties adopted to determine the structure-dependent coefficients $\mathbf{B}_1$ to $\mathbf{B}_3$ and the loading-dependent vector $\mathbf{p}_{i+1}$ are replaced by the updated structural properties for the current time step. As a result, both equations must be solved iteratively and thus an implicit implementation is required. Clearly, the performance of the implicit implementation of CDM might be drastically different from that of the explicit implementation of CDM for nonlinear systems. Since an implicit implementation will involve nonlinear iterations, it is time consuming in contrast to an explicit implementation. In addition to computational efficiency, stability and accuracy are also closely related to the performance of CDM-I. It is straightforward to prove that CDM-I with $\sigma = 1$ can have an unconditional stability for any structural systems and any viscous damping if a perfect iteration is achieved for each time step. Hence, it is evident that there is no need to apply a stability amplification factor to enlarge an unconditional stability range for CDM-I. On the other hand, to examine the difference in numerical accuracy between explicit and implicit implementations, variations of relative period errors with $\Delta t/T_0$ are plotted in Fig. 11.

It is seen in Figs. 11(a) and (c) that CDM-I and CDM-E generally has a small period distortion as $\Delta t/T_0 \le 0.05$ and the difference between both integration methods is not very significant. This difference originates from the difference in denominator of $\mathbf{B}_1$ to $\mathbf{B}_3$ and $\mathbf{p}_{i+1}$. In fact, for CDM-E, the denominator is $1-\alpha+\gamma 2\xi\Omega_0+\beta\Omega_0^2$ while for CDM-I it becomes $1-\alpha+\gamma 2\xi\Omega_{i+1}+\beta\Omega_{i+1}^2$. Since Ω_{i+1} is close to Ω_0 and both are very small for low frequency modes, thus, the denominator is dominated by $1-\alpha$ and then a small difference in period distortion is expected. On the other hand, a large difference will be found for high frequency modes between the two different implementations. However, there is no attempt to accurately integrate high frequency modes since they contribute insignificantly to a total response for an inertial problem. Notice that the only requirement for high frequency modes is no numerical instability. Besides, it is found that CDM-E shows less period distortion than that of CDM-I for stiffness softening systems while contrary conclusions are found for stiffness hardening systems. Notice that the curves for linear elastic systems coincided together for CDM-E and CDM-I. Fig. 11(b) reveals that CDM-E and CDM-I have no numerical damping for $\alpha = 0$. Whereas, for $\alpha = -0.5$, they can have favorable numerical damping as shown in Fig. 11(d).

Although CDM-E cannot have an unconditional stability for any structural systems, i.e., any δ_{i+1} value, it can have an unconditional stability range of $\delta_{i+1} \le 2$, which is large enough for practical applications. Meanwhile, it can have a comparable accuracy as that of CDM-I. The most important characteristic is that it can combine unconditional stability and explicit formulation together at the same time and thus CDM-E is more computationally efficient than for CDM-I

Table 1 Four specific members of CDM

Member	α	σ	Unconditional Stability Range		Numerical Dissipation
			CDM-E	CDM-I	
CDM1	0.0	1	$\delta_{i+1} \le 1$	$0 < \delta_{i+1} < \infty$	No
CDM2	–0.5	1	$\delta_{i+1} \le 1$	$0 < \delta_{i+1} < \infty$	Yes
CDM3	0.0	2	$\delta_{i+1} \le 2$	NA	No
CDM4	–0.5	2	$\delta_{i+1} \le 2$	NA	Yes

due to no nonlinear iterations for each time step. As a result, an explicit implementation of CDM is preferred over its implicit implementation. Hence, an explicit implementation of SDIMs is very promising for solving inertial problems. The application of the initial structural properties to replace the current structural properties for determining structure-dependent coefficients thoroughly explains why SDIMs can effectively overcome the Dahlquist barrier (Dahlquist 1956, 1963), which has been claimed by Dahlquist that no explicit method among the linear multi-step methods is absolutely stable.

8. Numerical examples

An application of CDM to solve some structural dynamic problems will be conducted in the following numerical study. The numerical examples are intentionally designed to affirm the numerical properties of CDM, such as the unconditional stability, controllable numerical dissipation and comparable accuracy in contrast to the conventional integration methods with a second-order accuracy, such as the constant average acceleration method (AAM) and WBZ-α method. Besides, the computational efficiency of CDM-E and CDM-I is also explored and is compared to that of the WBZ-α method. The specified values of α and σ corresponding to CDM1 to CDM4 are defined in Table 1 for brevity. In addition, their unconditional stability range and the numerical damping property are also shown in this table for comparison. There is no need to define CDM3-I and CDM4-I since an implicit implementation of CDM can have an unconditional stability for any $0 < \delta_{i+1} < \infty$ and thus $\sigma = 1$ is always taken.

8.1 Duffing equation

The Duffing equation is generally a non-linear second-order differential equation used to model certain damped and driven oscillators and thus is chosen for this study. It can generally describe the motion of a damped oscillator with a more complex potential than in simple harmonic motion. A simplified Duffing equation is considered and is:

$$\ddot{u} + \left(1 + u^2\right)u = \cos\left(\bar{\omega}t\right) \tag{34}$$

The stiffness of the system will be hardening after it deforms. The initial structural period is found to be 2πs for the system. The driving frequency $\bar{\omega}$ is taken as 0.2 rad/s and a zero initial condition is assumed.

Numerical solutions of the Duffing equation are shown in Fig. 12(a) and the time histories of instantaneous degree of nonlinearity are plotted in Fig. 12(b). Notice that AAM with $\Delta t = 0.01s$ is used to solve this equation and is considered as a reference solution for comparison. Meanwhile, AAM, CDM1-I and CDM3-E with $\Delta t = 0.2$s are also adopted to calculate the numerical solutions. Since the Duffing equation is only a single degree of freedom system, there is no high frequency mode and thus CDM1-I and CDM3-E are chosen to compute the responses. Fig. 12(a) shows that the results obtained from CDM1-I and CDM3-E are reliable and overlap the results obtained from AAM, which is a very commonly used implicit integration method. Besides, it is revealed by Fig. 12(b) that the system is encountered an instantaneous stiffness hardening case for each time step since δ_i varies between 1 and 1.75. Consequently, it can be concluded that CDM3-E can have a comparable accuracy with that of AAM and CDM1-I for such a highly nonlinear stiffness hardening system although it does not involve any nonlinear iterations for each time step.

8.2 An elastic pendulum

An elastic pendulum, as shown in Fig. 13, is considered. The instantaneous length of the pendulum can be calculated by $e = \sqrt{(u_1)^2 + (u_2)^2}$ and an unstretched pendulum length is e_0. The tangent stiffness matrix for the system (Geradin and Rixen 1994) can be expressed as:

$$\mathbf{K} = k\begin{bmatrix} 1 - \frac{1}{e}e_0 + \frac{1}{e^3}e_0 u_1^2 & \frac{1}{e^3}e_0 u_1 u_2 \\ \frac{1}{e^3}e_0 u_1 u_2 & 1 - \frac{1}{e}e_0 + \frac{1}{e^3}e_0 u_2^2 \end{bmatrix} \tag{35}$$

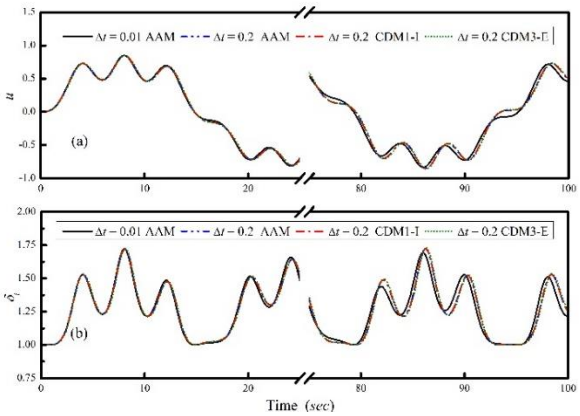

Fig. 12 Numerical solutions for Duffing equation

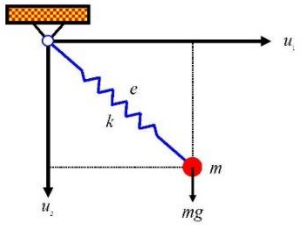

Fig. 13 A simple elastic pendulum

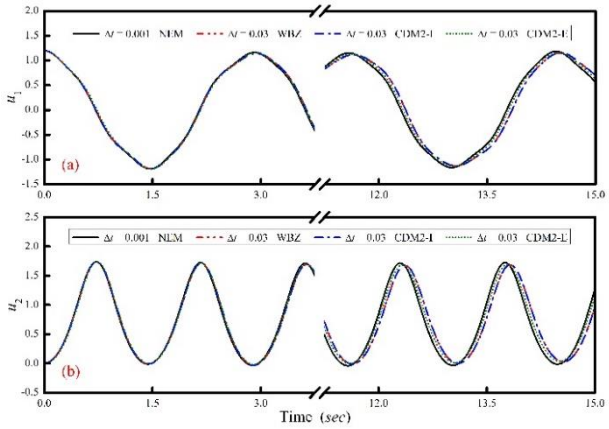

Fig. 14 Displacement response to a simple elastic pendulum

In this example $m = 1\,\text{kg}$, $k = 100\,\text{N/m}$, $e_0 = 1\,\text{m}$ and $g = 10\,\text{m/s}^2$ are taken. A highly nonlinear system can be simulated if the elastic pendulum has a large deformation in its axial direction. The initial conditions of $u_1(0) = 1.2\,\text{m}$, $u_2(0) = 0$, $\dot{u}_1(0) = 0$ and $\dot{u}_2(0) = 0$ are taken for each analysis. The result obtained from NEM with $\Delta t = 0.0001\text{s}$ is considered as a reference solution. In addition, WBZ with $\alpha = -\frac{1}{2}$, CDM2-I and CDM2-E are also used to calculate the responses by using $\Delta t = 0.02ss$ and the results are plotted in Fig. 14. Both CDM2-I and CDM2-E can have comparable results as those obtained from WBZ. Clearly, either explicit or implicit implementation of CDM can provide reliable solutions for the highly nonlinear system.

8.3 A five-story building

A 5-story building is considered for illustrating that CDM can have high-frequency numerical damping. Hence, this building is intentionally designated to have a relative high frequency mode. On the other hand, the stiffness of each story consists of a linear part and a nonlinear part so that different stiffness types can be simulated. A constant stiffness is taken for the linear part and the nonlinear part is assumed to be a function of the story drift. Consequently, the explicit expression of the stiffness for each story is:

$$k_j = k_{0-j}\left(1 + s_j\sqrt{|\Delta u_j|}\right) \tag{36}$$

where k_{0-j} denotes the initial stiffness, s_j is a constant and $\Delta u_j = u_j - u_{j-1}$ for $j = 1,2,\cdots,5$ is a story drift at the $j-th$ story. The shear-beam type building and its vibration properties are shown in Fig. 15. As a result, the initial natural frequencies of the lowest and highest modes for this building are found to be 6.16 and 2010 rad/s.

In Eq. (36), the instantaneous stiffness k_j can be less than, equal to or greater than the initial stiffness if s_j is chosen to be a negative, zero or positive value, respectively. In this study, two different types of stiffness properties are simulated for the 5-story building by means of using different s_j values. The simulation details are:

B$_1$ $s_j = -1.0$ a system with $\delta_{i+1} < 1$ for each mode

B$_2$ $s_j = 1.0$ a system with $\delta_{i+1} > 1$ for each mode

The free vibration responses to B$_1$ and B$_2$ are computed and are used to examine the effectiveness of the high-frequency numerical dissipation for CDM. The following two initial conditions are considered:

$$\text{I}_1 \quad \mathbf{u}(0) = \boldsymbol{\phi}_1/10 \quad \text{and} \quad \dot{\mathbf{u}}(0) = \mathbf{0}$$

$$\text{I}_2 \quad \mathbf{u}(0) = (\boldsymbol{\phi}_1 + \boldsymbol{\phi}_5)/10 \quad \text{and} \quad \dot{\mathbf{u}}(0) = \mathbf{0}$$

where $\boldsymbol{\phi}_1$ and $\boldsymbol{\phi}_5$ are shown in Fig. 15. Notice that I$_1$ only contains the pure first mode while I$_2$ consists of the first and fifth modes with equal weight.

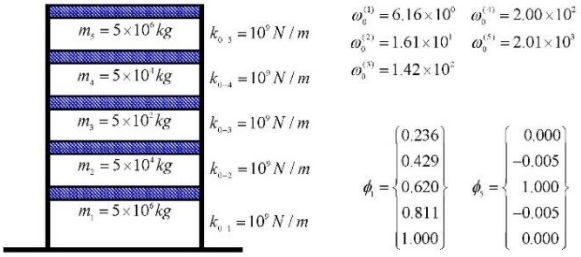

Fig. 15 A 5-story building and its vibration properties

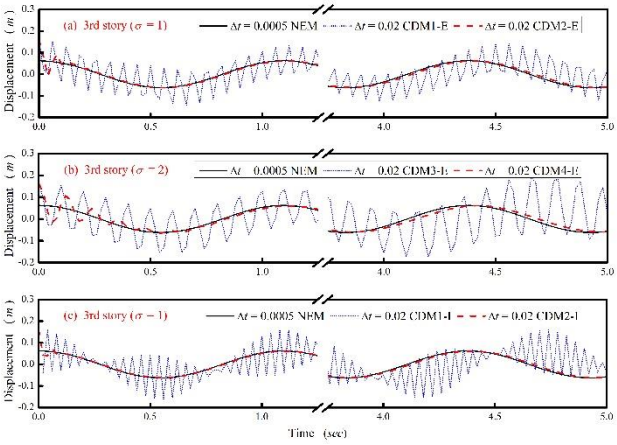

Fig. 16 Free vibration responses to B$_1$ (a stiffness softening system)

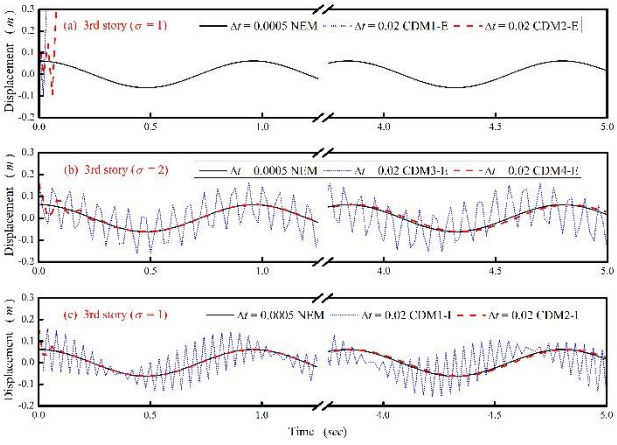

Fig. 17 Free vibration responses to B$_2$ (a stiffness hardening system)

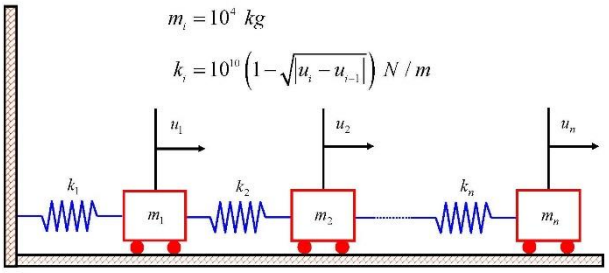

Fig. 18 A n-degree-of-freedom spring-mass system

Table 2 The lowest and highest natural frequencies and time integration data

n	$\omega_0^{(1)}(rad/s)$	$\omega_0^{(n)}(rad/s)$	a_g(m/s^2)	$\Delta t(s)$	t_d (s)	$t_d/\Delta t$
200	7.83	2000.00	12.5	0.02	4	200
400	3.92	2000.00	3.00	0.04	8	200
800	1.96	2000.00	0.75	0.08	16	200
1600	0.98	2000.00	0.20	0.16	32	200

At first, NEM with $\Delta t = 0.0005$s is applied to calculate the free vibration response to I_1 and the calculated result is considered as a reference solution. This small step size is chosen to meet the upper stability limit $\omega_0^{(5)}(\Delta t) = 1.01 < 2$ and thus a stable solution can be achieved. Notice that this time step is also small enough to accurately integrate the first mode. Meanwhile, the free vibration responses to I_2 are computed by CDM1-E to CDM4-E and CDM1-I to CDM2-I with $\Delta t = 0.02$s for both B_1 and B_2. Notice that CDM1-E, CDM1-I and CDM3-E possess no numerical damping while CDM2-E, CDM2-I and CDM4-E can have high frequency numerical damping. The calculated results for B_1 and B_2 are shown in Figs.16 and 16, respectively. It is revealed by ϕ_5, as shown in Fig.15, that the fifth mode only significantly contributes to the 3rd story while for the other stories its contribution is insignificant. This implies that the fifth modal response will only significantly appear in the displacement response of the 3rd story. Hence, the displacement response of the 3rd story is plotted in each plot of the both figures. In the following discussions, the response contribution from $\phi_5/10$ is treat as the source of the spurious oscillations and the period of this mode will be significantly distorted due to a relatively large value of $\Delta t/T_0^{(5)} = 6.4$, where $T_0^{(5)}$ is the structural period of the 5th mode.

8.4 A spring-mass system

Since CDM can be explicitly and implicitly implemented, it is of great interest to explore the computational efficiency between the two implementations. For this purpose, a system with a large degree of freedom will be considered. Besides, the system must be easily constructed and the number of the degree of freedom can be easily specified. As a result, a spring-mass system is designed and is shown in Fig. 18, where the spring stiffness k_i will decrease after the system deforms due to the nonlinear term $-10^{10}\sqrt{|u_i - u_{i-1}|}$. Thus, the case of $\delta_i \leq 1$ is found for each mode at each time step.

Four different n values of 200, 400, 800 and 1600 are specified and thus the four systems with the degrees of freedom of 200, 400, 800 and 1600 are simulated. Each system is excited by a constant acceleration at its base. The choice of a constant load is intended to avoid the difficulty to faithfully seize the dynamic loading. The lowest and highest initial natural frequencies and the time integration data for each system are listed in Table 2. A total number of 200 steps is performed for each analysis. Four integration methods of NEM, WBZ with $\alpha = -0.5$, CDM2-I and CDM2-E are used to calculate the responses. Since NEM is conditionally stable, the time step must be chosen to meet the conditional stability. As a result, $\Delta t = 0.001s$ is chosen for each system since the highest initial natural frequency of each system is as large as 2000 rad/s, which is shown in Table 2. Numerical solutions obtained from this time step can be considered as reference solutions for the four systems since this time step is much smaller than that required by accuracy consideration. On the other hand, WBZ, CDM2-I and CDM2-E all can have an unconditional stability and thus the step size for time integration is selected based on accuracy consideration. For each system, the step size Δt to perform time integration for using WBZ, CDM2-I and CDM2-E, the loading duration t_d and the total number of steps $t_d/\Delta t$ are also listed in Table 2.

The displacement responses of the four systems are shown in Fig. 19. Comparing the results obtained from WBZ, CDM2-I and CDM2-E to the reference solutions for each plot of this figure, the time steps of $\Delta t = 0.02$, 0.04, 0.08 and 0.16s seem to be the maximum allowable time steps to yield acceptable solutions corresponding to the 200-DOF, 400-DOF, 800-DOF and 1600-DOF systems. The calculated results obtained from CDM2-I and CDM2-E almost coincide those obtained from WBZ for the four systems. This attests that CDM can have comparable accuracy when compared to WBZ. On the other hand, the unconditional stability of CDM is also indicated since the value of $\omega_0^{(n)}(\Delta t)$ is as large as 40, 80, 160 and 320 in correspondence to the 200-DOF, 400-DOF, 800-DOF and 1600-DOF systems.

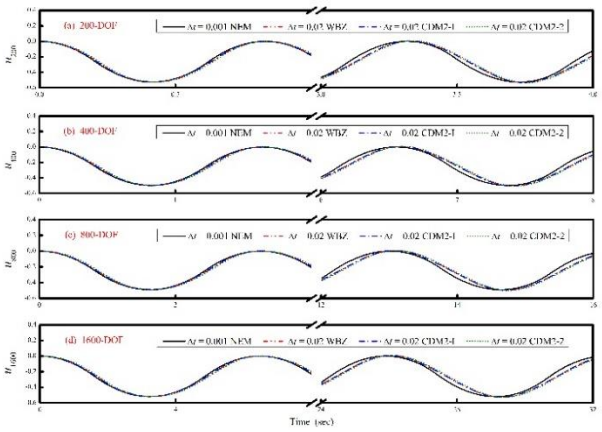

Fig. 19 Displacement responses of spring-mass systems

Table 3 Comparisons of CPU time

N-DOF	NEM	WBZ	CDM2-I	CDM2-E	$\frac{\text{CDM2-E}}{\text{NEM}}$	$\frac{\text{CDM2-E}}{\text{WBZ}}$	$\frac{\text{CDM2-E}}{\text{CDM2-I}}$
200	2.85	20.98	20.97	0.20	0.070	0.0095	0.0095
400	28.92	172.02	172.27	0.98	0.034	0.0057	0.0057
800	395.08	1883.00	1857.58	6.48	0.016	0.0034	0.0035
1600	5628.97	16833.41	16756.23	12.58	0.0076	0.0025	0.0025

Table 4 Comparisons of dissipative SDIMs

Property	C-1	C-2	KRM	CDM
Unconditional Stability	Yes	Yes	Yes	Yes
Second-order accuracy	Yes	Yes	Yes	Yes
Explicit formulation	Yes	Yes	Yes	Yes
Controllable numerical responses	Yes	Yes	Yes	Yes
Overshoot in transient responses	No	No	No	No
Overshoot it steady-state responses	Yes	Yes	Yes	No
Self-starting	No	No	Yes	Yes
Weak instability	No	No	Yes	No

C-1 The first family of Chang dissipative structure-dependent integration method (Chang 2014a)
C-2 The second family of Chang dissipative structure-dependent integration method
KRM = The dissipative structure-dependent integration method developed by Kolay and Ricles (2014).

To evaluate the computational efficiency of CDM-I and CDM-E, the consumed CPU time for each dynamic analysis is recorded and listed in Table 3 for NEM, WBZ, CDM2-I and CDM2-E. The 5th column shows that CDM2-E involves much less computational efforts when compared to NEM, WBZ and CDM2-I. Apparently, NEM is inappropriate for solving an inertial problem since a small step size is required to satisfy stability conditions. Thus, it costs a large CPU time for each system. On the other hand, a large time step can be adopted for WBZ, CDM2-I and CDM2-E based on accuracy consideration due to unconditional stability. Since WBZ and CDM2-I are implicitly implemented and they consume many and roughly the same computational efforts as shown in the 3rd and 4th columns. This is because an iteration procedure is needed in each time step and it is very time consuming for a matrix of large order. Clearly, CDM2-E can combine explicit formulation and unconditional stability together and thus CDM2-E can save many computational efforts. It is found in the last three columns that the computational efficiency of CDM2-E will increase as the total number of the degrees of freedom increases. Notice that the CPU time consumed by CDM2-E is only about 0.25% of that consumed by WBZ and CDM2-I for the 1600-DOF system.

9. Conclusions

The application of an eigen-based theory to develop a novel family of dissipative SDIMs is presented in this work. The successful development of this dissipative integration method can be applied to affirm the feasibility of the eigen-based theory for developing a general SDIM. In addition, a canonical procedure is constructed for developing a SDIM that can have desired numerical properties. At first, an eigen-decomposition technique can be employed to decompose a coupled equation of motion into a series of uncoupled modal equations of motion. Then, an eigen-dependent integration method is proposed to solve each modal equation of motion. Subsequently, all the eigen-dependent integration methods are converted into a SDIM. Some key issues and techniques are involved in this development so that an improved SDIM is derived, such as the adoptions of an asymptotic equation of motion, a conversion of a two-step difference equation to a one-step difference equation, an appropriately assumed displacement difference equation, a stability amplification factor and a loading-correction term. Thus, a new dissipative SDIM is developed and it has desired numerical properties. To confirm the superiority of this SDIM over other SDIMs, the major properties of the four dissipative SDIMs are listed in Table 4. Clearly, these four integration methods can have the same first five numerical properties while they are different for the last three numerical properties. The defects for C-1 and C-2 are the adverse overshoot in high frequency steady-state responses and no capability of self-starting while the critical drawbacks of KRM are a weak instability and an adverse overshoot in high frequency steady-state responses. Clearly, the novel family of the SDIMs does not possess any adverse numerical properties. Besides, it is computationally efficient in the solution of inertia problems in contrast to conventional dissipative integration methods, such as HHT, WBZ and the generalized-a method, due to no involvement of nonlinear iterations for each step.

It is verified that the proposed family of SDIMs can have an explicit implementation if the initial structural properties are adopted to calculate the structure-dependent coefficients while it can be also implicitly implemented if the structure-dependent coefficients are updated with the current structural properties for each time step. Both implementations can have the same numerical properties except for stability property. An implicit implementation can have unconditional stability for any structural systems if a perfect iteration is achieved for each time step. On the other hand, an explicit implementation can generally have an unconditional stability for linear elastic and stiffness

softening systems. Notice that although it only has a conditional stability for stiffness hardening systems, an appropriate stability amplification factor can be applied to enlarge an unconditional stability range so that it can also have an unconditional stability for the stiffness hardening systems of practical significance. An explicit implementation will not involve any nonlinear iterations and thus it is more computational efficient than for an implicit implementation since it can simultaneously combine unconditional stability and explicit formulation. Thus, an explicit implementation is preferred over an implicit implementation. In general, the choice of $-1 \leq \alpha \leq 0$, $\beta = \frac{1}{4}(1-\alpha)^2$ and $\gamma = \frac{1}{2} - \alpha$ is strongly recommended for practical applications. On the other hand, $\sigma = 1$ can be taken if it is known as a priori that there experiences no stiffness hardening for the analyzed system. Otherwise, $\sigma = 2$ must be chosen.

Acknowledgments

The author is grateful to acknowledge that this study is financed by the Ministry of Science and Technology, Taiwan, R.O.C., under Grant No. MOST-107-2221-E-027-011.

References

Alamatian, J. (2013), "New implicit higher order time integration for dynamic analysis", *Struct. Eng. Mech.*, **48**(5), 711-736. https://doi.org/ 10.12989/sem.2013.48.5.711

Armero, F. and Romero, I. (2001), "On the formulation of high-frequency dissipative time-stepping algorithms for non-linear dynamics. Part II: Second-order methods", *Comput. Methods Appl. Mech. Eng.*, **190**, 6783-6824. https://doi.org/ 10.1016/S0045-7825(01)00233-X

Belytschko, T. and Hughes, T.J.R. (1983), *Computational Methods for Transient Analysis*, Elsevier Science Publishers B.V., North-Holland, Amsterdam.

Chang, S.Y. (1997), "Improved numerical dissipation for explicit methods in pseudodynamic tests", *Earthq. Eng. Struct. Dynam.*, **26**, 917-929. https://doi.org/10.1002/(SICI)1096-9845(199709)26:9<917:AID-EQE685>3.0.CO;2-9

Chang, S.Y. (2000), "The γ-function pseudodynamic algorithm", *J. Earthq. Eng.*, **4**(3), 303-320. https://doi.org/10.1080/13632460009350373

Chang, S.Y. (2001), "Analytical study of the superiority of the momentum equations of motion for impulsive loads", *Comput. Struct.,* **79**(15), 1377-1394. https://doi.org/10.1016/S0045-7949(01)00044-X.

Chang, S.Y. (2002), "Explicit pseudodynamic algorithm with unconditional stability", *J. Eng. Mech. ASCE*, **128**(9), 935-947. https://doi.org/10.1061/(ASCE)0733-9399(2002)128:9(935).

Chang, S.Y. (2006), "Accurate representation of external force in time history analysis", *J. Eng. Mech. ASCE*, **132**(1), 34-45. https://doi.org/10.1061/(ASCE\)0733-9399(2006)132:1(34).

Chang, S.Y. (2007), "Improved explicit method for structural dynamics", *J. Eng. Mech. ASCE*, **133**(7), 748-760. https://doi.org/10.1061/(ASCE)0733-9399(2007)133:7(748).

Chang, S.Y. (2009), "An explicit method with improved stability property", *J. Numerical Method Eng.*, **77**(8), 1100-1120. https://doi.org/10.1002/nme.2452.

Chang, S.Y. (2010), "A new family of explicit method for linear structural dynamics", *Comput. Struct.*, **88**(11-12), 755-772. https://doi.org/10.1016/j.compstruc.2010.03.002.

Chang, S.Y. (2014a), "A Family of non-iterative integration methods with desired numerical dissipation", *J. Numerical Methods Eng.*, **100**(1), 62-86. https://doi.org/10.1002/nme.4720.

Chang, S.Y. (2014b), "Family of structure-dependent explicit methods for structural dynamics", *J. Eng. Mech. ASCE*, **140**(6). https://doi.org/10.1061/(ASCE)EM.1943-7889.0000748.

Chang, S.Y. (2015a), "Discussion of paper 'Development of a family of unconditionally stable explicit direct integration algorithms with controllable numerical energy dissipation' by Chinmoy Kolay and James M. Ricles, *Earthquake Engineering and Structural Dynamics* 2014; 43: 1361–1380," *Earthq. Eng. Struct. Dynam.*, **44**(2), 325-328. https://doi.org/10.1002/eqe.2514.

Chang, S.Y. (2015b), "Dissipative, non-iterative integration algorithms with unconditional stability for mildly nonlinear structural dynamics", *Nonlinear Dynamics*, 79(2), 1625-1649. https://doi.org/10.1007/s11071-014-1765-7.

Chang, S.Y. (2015c), "A general technique to improve stability property for a structure-dependent integration method", *J. Numerical Methods Eng.*, **101**(9), 653-669. https://doi.org/10.1002/nme.4806.

Chang, S.Y. (2017), "Assessments of dissipative structure-dependent integration methods", *Struct. Eng. Mech.*, **62**(2), 151-162. https://doi.org/10.12989/sem.2017.62.2.151.

Chang, S.Y. (2018a), "Performances of non-dissipative structure-dependent integration methods," *Struct. Eng. Mech.*, **65**(1), 91-98. https://doi.org/ 10.12989/sem.2018.65.1.091.

Chang, S.Y. (2018b), "Elimination of overshoot in forced vibration response for Chang explicit family methods", *J. Eng. Mech. ASCE*, **144**(2). https://doi.org/10.1061/(ASCE)EM.1943-7889.0001401.

Chang, S.Y., (2018c), "An unusual amplitude growth property and its remedy for structure-dependent integration methods", *Comput. Methods Appl. Mech. Eng.*, **330**, 498-521. https://doi.org/10.1016/j.cma.2017.11.012.

Chang, S.Y. and Mahin, S.A. (1993), "Two new implicit algorithms of pseudodynamic test methods," *J. Chinese Institute Eng.*, **16**(5), 651-664. https://doi.org/10.1080/02533839.1993.9677539.

Chang, S.Y., Wu, T.H. and Tran, N.C. (2015), "A family of dissipative structure-dependent integration methods", *Struct. Eng. Mech.*, **55**(4), 815-837. https://doi.org/10.12989/sem.2015.55.4.815.

Chang, S.Y., Wu, T.H. and Tran, N.C. (2016), "Improved formulation for a structure-dependent integration method", *Struct. Eng. Mech.*, **60**(1), 149-162. https://doi.org/10.12989/sem.2016.60.1.149.

Chang, S.Y. (2019). "A dual family of dissipative structure-dependent integration methods for structural nonlinear dynamics", *Nonlinear Dynam.*, **98**(1), 703-734. https://doi.org/ 10.1007/s11071-019-05223-y.

Chung, J. and Hulbert, G.M. (1993), "A time integration algorithm for structural dynamics with improved numerical dissipation: the generalized-α method", *J. Appl. Mech.*, **60**(6), 371-375. https://doi.org/10.1115/1.2900803.

Chen, C. and Ricles, J.M. (2008), "Development of direct integration algorithms for structural dynamics using discrete control theory", *Earthq. Eng. Struct. Dynam.*, **134**(8), 76-683. https://doi.org/ 10.1061/(ASCE)0733-9399(2008)134:8(676).

Civalek, O. (2007), "Nonlinear dynamic response of MDOF systems by the method of harmonic differential quadrature (HDQ)", *Struct. Eng. Mech.*, **25**(2), 201-217. https://doi.org/ 10.12989/sem.2007.25.2.201.

Clough, R. and Penzien, J. (2003), *Dynamics of Structures*, Third

Edition, Mcgraw-Hill, USA.

Dahlquist, G. (1956), "Convergence and stability in the numerical integration of ordinary differential equations", *Mathematica Scandinavica*, **4**, 33-53. https://doi.org/ https://doi.org/10.7146/math.scand.a-10454.

Dahlquist, G. (1963), "A special stability problem for linear multistep methods", *BIT*, **3**, 27-43. https://doi.org/10.1007/BF01963532.

Du, X., Yang, D., Zhou, J., Yan, X., Zhao, Y. and Li, S. (2018), "New explicit integration algorithms with controllable numerical dissipation for structural dynamics", *J. Struct. Stability Dynam.*, **18**(3), 1850044. https://doi.org/ 10.1142/S021945541850044X

Gao, Q., Wu, F., Zhang, H.W., Zhong, W.X., Howson, W.P. and Williams, F.W. (2012), "A fast precise integration method for structural dynamics problems", *Struct. Eng. Mech.*, **43**(1), 1-13. https://doi.org/ 10.12989/sem.2012.43.1.001

Geradin, M. and Rixen, D. (1994), *Mechanical Vibrations Theory and Application to Structural Dynamics*, John Wiley and Sons Inc., USA.

Goudreau, G.L. and Taylor, R.L. (1972), "Evaluation of numerical integration methods in elasto-dynamics", *Computer Methods in Applied Mechanics and Engineering*, 2, 69-97. https://doi.org/10.1016/0045-7825(73)90023-6.

Gui, Y., Wang, J.T., Jin, F., Chen, C. and Zhou, M.X. (2014), "Development of a family of explicit algorithms for structural dynamics with unconditional stability", *Nonlinear Dynam.*, **77**(4), 1157-1170. https://doi.org/ 10.1007/s11071-014-1368-3

Hadianfard, M.A. (2012), "Using integrated displacement method to time-history analysis of steel frames with nonlinear flexible connections", *Struct. Eng. Mech.*, **41**(5), 675-689. https://doi.org/ 10.12989/sem.2012.41.5.675

Har, J., and Tamma, K.K. (2012), *Advances in Computational Dynamics of Particles, Materials and Structures*, John Wiley and Sons Inc. https://doi.org/ 10.1002/9781119965893.

Hilber, H.M., Hughes, T.J.R. and Taylor, R.L. (1977), "Improved numerical dissipation for time integration algorithms in structural dynamics", *Earthq. Eng. Struct. Dynam.*, **5**, 283-292. https://doi.org/10.1002/eqe.4290050306.

Hilber, H.M. and Hughes, T.J.R. (1978), "Collocation, dissipation, and 'overshoot' for time integration schemes in structural dynamics", *Earthq. Eng. Struct. Dynam.*, **6**, 99-118. https://doi.org/10.1002/eqe.4290060111.

Hughes, T.J.R. (1987), *The Finite Element Method*, Prentice-Hall, Inc., Englewood Cliffs, N.J., U.S.A.

Kim, W. and Lee, J.H. (2018), "An improved explicit time integration method for linear and nonlinear structural dynamics", *Comput. Struct.*, **206**, 42-53. https://doi.org/ 10.1016/j.compstruc.2018.06.005

Kim, W. and Choi, S.Y. (2018), "An improved implicit time integration algorithm: The generalized composite time integration algorithm", *Comput. Struct.*, **196**, 341-354. https://doi.org/ 10.1016/j.compstruc.2017.10.002.

Kim, W. (2019), "A simple explicit single step time integration algorithm for structural dynamics", *J. Numerical Method Eng.*, 1-21. https://doi.org/ 10.1002/nme.6054

Kolay, C. and Ricles, J.M. (2014), "Development of a family of unconditionally stable explicit direct integration algorithms with controllable numerical energy dissipation", *Earthq. Eng. Struct. Dynam.*, **43**, 1361-1380. https://doi.org/ 10.1002/eqe.2401.

Lax, P.D. and Richmyer, R.D. (1956) "Survey of the stability of linear difference equations", *Communications on Pure and Appl. Math.*, **9**, 267-293. https://doi.org/ 10.1007/0-387-28148-7_11.

Newmark, N.M. (1959), "A method of computation for structural dynamics", *J. Eng. Mech. Division*, ASCE, **85**(3), 67-94.

Park, K.C. (1975), "An improved stiffly stable method for direct integration of nonlinear structural dynamic equations", *J. Appl. Mech.*, **42**, 464-470. https://doi.org/10.1115/1.3423600.

Rezaiee-Pajand, M., Esfehani, S.A.H. and Karimi-Rad, M. (2018) "Highly accurate family of time integration method", *Struct. Eng. Mech.*, **67**(6), 603-614. https://doi.org/ 10.12989/sem.2018.67.6.603.

Shojaee, S., Rostami, S. and Abbasi, A. (2015), "An unconditionally stable implicit time integration algorithm: Modified quartic B-spline method", *Comput. Struct.*, **153**, 98-111. https://doi.org/ 10.1016/j.compstruc.2015.02.030

Soares, D. (2014), "An explicit family of time marching procedures with adaptive dissipation control", *J. Numerical Methods Eng.*, **100**, 165-182. https://doi.org/ 10.1002/nme.4722

Su, C. and Xu, R. (2014), "Random vibration analysis of structures by a time-domain explicit formulation method", *Struct. Eng. Mech.*, **52**(2), 239-260. https://doi.org/ 10.12989/sem.2014.52.2.239

Tang, Y. and Lou, M.L. (2017), "New unconditionally stable explicit integration algorithm for real-time hybrid testing", *J. Eng. Mech.*, **143**(7), 04017029. https://doi.org/ 10.1061/(ASCE)EM.1943-7889.0001235.

Wen, W.B., Wei, K., Lei, H.S., Duan, S.Y. and Fang, Y.N. (2017), "A novel sub-step composite implicit time integration scheme for structural dynamics", *Comput. Struct.*, **172**, 176-186. https://doi.org/ 10.1016/j.compstruc.2016.11.018

Wilson, E.I. Farhoomand, I. and Bathe, K.J. (1973), "Nonlinear dynamic analysis of complex structures", *Earthq. Eng. Struct. Dynam.*, **1**, 241-252. https://doi.org/10.1002/eqe.4290010305

Wood, W.L., Bossak, M. and Zienkiewicz, O.C. (1981), "An alpha modification of Newmark's method", *J. Numerical Methods Eng.*, **15**, 1562-1566. https://doi.org/ 10.1002/nme.1620151011

Xing, Y., Ji, Y. and Zhang, H. (2019) "On the construction of a type of composite time integration methods", *Comput. Struct.*, **221**, 157-178. https://doi.org/ 10.1016/j.compstruc.2019.05.019

Zhou, X, Tamma, K.K. (2004), "Design, analysis, and synthesis of generalized single step single solve and optimal algorithms for structural dynamics." *J. Numerical Methods Eng.*, **59**, 597–668. https://doi.org/ 10.1002/nme.873

CC